Article

Cell Reports

Blocking Antibodies Targeting the CD39/CD73 Immunosuppressive Pathway Unleash Immune Responses in Combination Cancer Therapies

Graphical Abstract

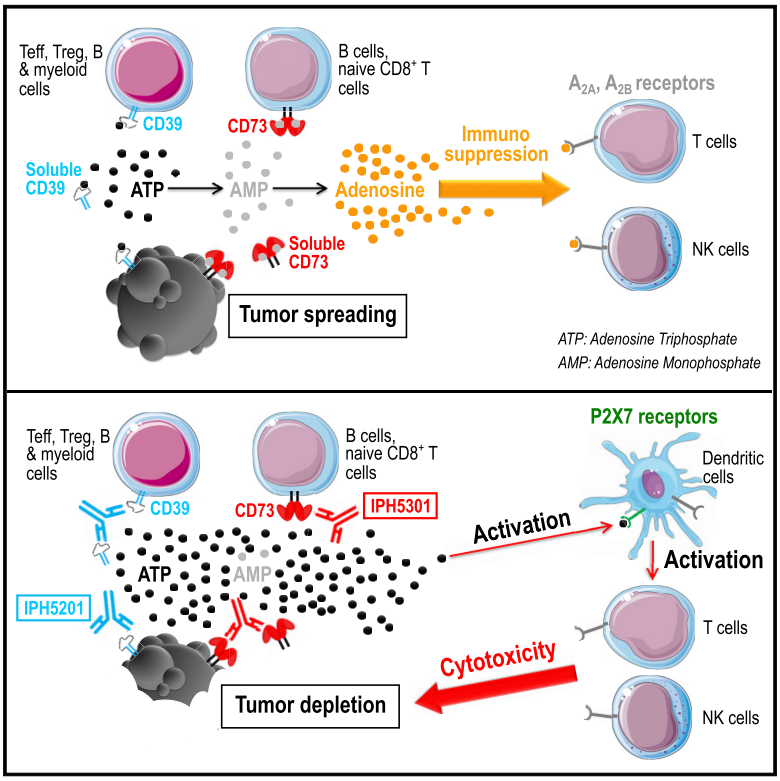

Highlights

- IPH5201 and IPH5301 block cell-borne and soluble CD39 and CD73, respectively
- IPH5201 maintains immunogenic extracellular ATP
- When used in combination with chemotherapy, IPH5201 promotes antitumor immunity
- Targeting CD39 and CD73 synergistically promotes cancer patient T cell activation

Authors

Ivan Perrot, Henri-Alexandre Michaud, Marc Giraudon-Paoli, ..., Eric Vivier, Carine Paturel, Nathalie Bonnefoy

Correspondence

vivier@ciml.univ-mrs.fr (E.V.), carine.paturel@innate-pharma.fr (C.P.), nathalie.bonnefoy@inserm.fr (N.B.)

In Brief

The production of adenosine via CD39 and CD73 ectoenzymes participates in an immunosuppressive tumor microenvironment. Perrot et al. generated two antibodies, IPH5201 and IPH5301, targeting human CD39 and CD73, respectively. *In vitro* and *in vivo* data support the use of anti-CD39 and anti-CD73 mAbs in combination cancer therapies.

Perrot et al., 2019, Cell Reports *27*, 2411–2425
May 21, 2019
https://doi.org/10.1016/j.celrep.2019.04.091

CellPress

Cell Reports
Article

Blocking Antibodies Targeting the CD39/CD73 Immunosuppressive Pathway Unleash Immune Responses in Combination Cancer Therapies

Ivan Perrot,[1,11] Henri-Alexandre Michaud,[2,11] Marc Giraudon-Paoli,[1] Séverine Augier,[1] Aurélie Docquier,[3] Laurent Gros,[2] Rachel Courtois,[1] Cécile Déjou,[3] Diana Jecko,[1] Ondine Becquart,[2,4] Hélène Rispaud-Blanc,[1] Laurent Gauthier,[1] Benjamin Rossi,[1] Stéphanie Chanteux,[1] Nicolas Gourdin,[1] Beatrice Amigues,[5] Alain Roussel,[5] Armand Bensussan,[6] Jean-François Eliaou,[2,7] Jérémy Bastid,[3] François Romagné,[8] Yannis Morel,[1] Emilie Narni-Mancinelli,[9] Eric Vivier,[1,9,10,12,*] Carine Paturel,[1,11,*] and Nathalie Bonnefoy[2,11,*]

[1]Innate Pharma, 117 Avenue de Luminy, 13009 Marseille, France
[2]IRCM, Institut de Recherche en Cancérologie de Montpellier, INSERM U1194, Université de Montpellier, Institut régional du Cancer de Montpellier, 34298 Montpellier, France
[3]OREGA Biotech, 69130 Ecully, France
[4]Département de Dermatologie, Centre Hospitalier Régional Universitaire de Montpellier et Faculté de Médecine, Université de Montpellier, 34295 Montpellier, France
[5]CNRS, Aix Marseille Université, AFMB, Architecture et Fonction des Macromolécules Biologiques, 13009 Marseille, France
[6]Institut National de la Santé et de la Recherche Médicale (INSERM) UMR-S 976, Université Paris Diderot, Sorbonne Paris Cité, Laboratory of Human Immunology, Pathophysiology and Immunotherapy, 75475 Paris, France
[7]Département d'Immunologie, Centre Hospitalier Régional Universitaire de Montpellier et Faculté de Médecine, Université de Montpellier, 34295 Montpellier, France
[8]MI-mAbs, Aix Marseille Université, 117 Avenue de Luminy, 13009 Marseille, France
[9]Aix Marseille Université, INSERM, CNRS, Centre d'Immunologie de Marseille-Luminy, 13009 Marseille, France
[10]Service d'Immunologie, Marseille Immunopôle, Hôpital de la Timone, Assistance Publique-Hôpitaux de Marseille, 13005 Marseille, France
[11]These authors contributed equally
[12]Lead Contact
*Correspondence: vivier@ciml.univ-mrs.fr (E.V.), carine.paturel@innate-pharma.fr (C.P.), nathalie.bonnefoy@inserm.fr (N.B.)
https://doi.org/10.1016/j.celrep.2019.04.091

SUMMARY

Immune checkpoint inhibitors have revolutionized cancer treatment. However, many cancers are resistant to ICIs, and the targeting of additional inhibitory signals is crucial for limiting tumor evasion. The production of adenosine via the sequential activity of CD39 and CD73 ectoenzymes participates to the generation of an immunosuppressive tumor microenvironment. In order to disrupt the adenosine pathway, we generated two antibodies, IPH5201 and IPH5301, targeting human membrane-associated and soluble forms of CD39 and CD73, respectively, and efficiently blocking the hydrolysis of immunogenic ATP into immunosuppressive adenosine. These antibodies promoted antitumor immunity by stimulating dendritic cells and macrophages and by restoring the activation of T cells isolated from cancer patients. In a human CD39 knockin mouse preclinical model, IPH5201 increased the anti-tumor activity of the ATP-inducing chemotherapeutic drug oxaliplatin. These results support the use of anti-CD39 and anti-CD73 monoclonal antibodies and their combination with immune checkpoint inhibitors and chemotherapies in cancer.

INTRODUCTION

Over the last decade, the focus of cancer treatment has shifted from the tumor to the host, with the development of various forms of immune-based therapies that mobilize the immune system to promote or restore an effective antitumor immune response (Okazaki et al., 2013; Palucka and Coussens, 2016; Sharma and Allison, 2015a, 2015b). Unprecedented improvements in tumor control have been achieved with therapeutic blocking antibodies that release immune inhibitory "checkpoints" (immune checkpoint inhibitors [ICIs]). However, such treatments often yield sustained benefits, but strong responses are observed in only a minority of treated patients, whereas resistance to ICIs is observed in a substantial fraction of patients. Major efforts are therefore being made to identify new targets that activate, unleash, or enhance antitumor immune responses. In this context the targeting of the immunosuppressive tumor microenvironment (TME) may be of interest.

Cancer immune evasion largely involves the generation of high amounts of immunosuppressive adenosine (Ado) within the tumor environment. Purinergic signaling is involved in inflammation and cancer and plays a key role in modulating cell migration, proliferation, and death (de Andrade Mello et al., 2017). ATP and Ado released into the TME are among the most potent modulators of both tumor cell and immune responses. Apoptotic cells release ATP, which acts as a major signal, recruiting phagocytes and essential for the

immunogenicity of cancer-cell death (Silva-Vilches et al., 2018). ATP binds to type 2 purinergic/pyrimidinergic P2X and P2Y receptors and promotes dendritic cell (DC) maturation for antitumoral T cell priming. ATP also inhibits the proliferation of tumor cells, but not of healthy cells, and promotes the death of cancer cells. By contrast, Ado attenuates the immune response by suppressing effector cell function and stabilizing immunosuppressive regulatory T cells based on their expression of Ado A_{2x} receptors. Ado inhibits dendritic cell activation, Th1/Th2 cytokine production, T cell proliferation and activation, natural killer (NK)-cell activation, maturation, and cytotoxicity, and it enhances the suppressive functions of Tregs, Tr1 cells, and macrophages (de Andrade Mello et al., 2017). ATP and Ado local concentrations are tightly controlled by several ectonucleotidases, including CD39 (ectonucleoside triphosphate diphosphohydrolase 1, E-NTPDase1) and CD73 (ecto-5′-nucleotidase, Ecto5′NTase), expressed by cancer cells, immune cells, and the vasculature. CD39 is a plasma-membrane-bound enzyme that cleaves ATP and ADP down into AMP. AMP is converted into Ado by CD73 on the cell surface. This sequential activity of the CD39/CD73 pathway scavenges extracellular ATP and generates immunosuppressive Ado in the TME.

Early preclinical studies showed that CD39-deficient mice were resistant to tumor metastases in the B16F10 mouse model of melanoma and the MC-38 mouse model of colorectal cancer (Sun et al., 2010). CD39 expression on tumor and endothelial cells promotes angiogenesis and metastatic tumor spread, whereas CD39 expression on Tregs is crucial for suppressing NK cell antitumor activity (Jackson et al., 2007; Sun et al., 2013). CD39 overexpression in tumor-bearing mice increases the liver metastasis of MC-26 colorectal tumors in mice (Künzli et al., 2011), whereas pharmacological blockade of CD39 and other hydrolases such as E-NTPDase 2 and 3 with POM1 increases antitumor immunity and decreases metastatic spread in several tumor models (Sun et al., 2013). Furthermore, CD39 blockade enhances the immune cell effector response to human ovarian cancer cell lines and follicular lymphoma cells *in vitro* and promotes the survival of non-obese diabetic (NOD) mice in patient-derived sarcoma models (Häusler et al., 2014; Hayes et al., 2015; Hilchey et al., 2009). Thus, blocking CD39 activity may be an effective approach to limit the hydrolysis of immunogenic ATP and prevent the accumulation of immunosuppressive Ado. One anti-CD39 monoclonal antibody (mAb), BY40, has been generated and reported to block the activity of the membrane-associated, but not soluble, human CD39 enzyme (Nikolova et al., 2011), but its clinical efficacy has still not been evaluated.

Several preclinical studies have shown that host CD73 deficiency delays tumor growth in multiple models of syngeneic transplantable tumors. CD73-deficient mice are also resistant to lung metastasis after the intravenous injection of melanoma and prostate cancer cells (Stagg et al., 2011, 2012). Many approaches using antibodies against CD73 or inhibitors have shown large antitumor and anti-metastatic effects in several preclinical models (Antonioli et al., 2016, 2017). Given these promising results, four mAbs, MEDI9447, BMS986179, SRF373 (also known as NZV930), and CPI-006 (also known as CPX-006), inhibiting CD73 activity and/or inducing CD73 down modulation are currently under investigation in early-phase clinical trials.

We show here that CD39 deficiency enhances the benefits from combined cancer therapies in preclinical mouse solid tumor models of melanoma and fibrosarcoma. We report the generation and characterization of two blocking antibodies against human CD39 and CD73, referred to as IPH5201 and IPH5301, respectively. The anti-CD39 mAb IPH5201 blocked ATP hydrolysis by both membrane and soluble CD39, thereby promoting DC maturation and macrophage activation, whereas the anti-CD73 mAb IPH5301 blocked the degradation of AMP into immunosuppressive Ado and displays different functional characteristics over currently used mAbs. Both IPH5201 and IPH5301 prevented the Ado-mediated inhibition of T cells purified from patients with breast cancer or melanoma. The IPH5201 efficiently increased the anti-tumor activity of the ATP-inducing chemotherapeutic drug oxaliplatin in a mice tumor model. These data provide the scientific rationale for the clinical development of IPH5201 and IPH5301 and their use in innovative strategies of cancer immunotherapy.

RESULTS

CD39 Disruption Improves Antitumor Immunity

The tumor microenvironment can attenuate antitumor immunity by generating purinergic mediators. We investigated this phenomenon by monitoring the growth, in a mouse model of melanoma, of subcutaneously injected B16F10 cells in wild-type (WT) and CD39-deficient mice. B16F10 tumor growth was delayed and survival was prolonged in CD39-deficient as compared to WT animals (Figure 1A). The B16F10 melanoma cells do not express the CD39 ectonucleotidase per se even after engraftment in mice (Allard et al., 2014). We monitored the ATPase activity and the generation of AMP from added ATP within cells isolated from the tumor or the spleen of WT mice. AMP levels were lower in cells isolated from CD39-deficient mice (Figure S1A) and in the presence of ARL-67156, a chemical inhibitor of CD39 (data not shown), indicating that CD39 is the major enzyme involved in the ATP degradation by B16F10 tumor and spleen beds.

We next investigated CD39 expression in B16F10 tumor tissues. An average of 72.5% (45.3%–90.7%) of the $CD39^+$ cells were $CD45^+$ (Figure S1B), while engrafted B16F10 tumor cells did not express CD39 endogenously (Figure S1C). In contrast, engrafted B16F10 express CD73 that could reduce tumor growth control in CD39 knockout (KO) mice as AMP CD73 substrate can be generated independently of CD39 through other enzymes such as NPP1 or CD38. We further characterized immune cell infiltration and their expression of CD39 over time. Immune cell infiltrate was subjected to modifications from day 8 until day 21 post B16F10 grafting, characterized by an inversion of the lymphoid and myeloid frequencies between day 8 and day 21 (Figure S1D, left panel) and by a progressive increase of $CD39^+$ cells with tumor growth evolution (Figure S1D, right panel). The myeloid-derived suppressive cells (MDSCs), DCs, and macrophages that naturally expressed CD39 represented about 35% of the immune infiltrate at day 8 and 70% at day 21 (Figure S1D, left panel). At that time, they accounted

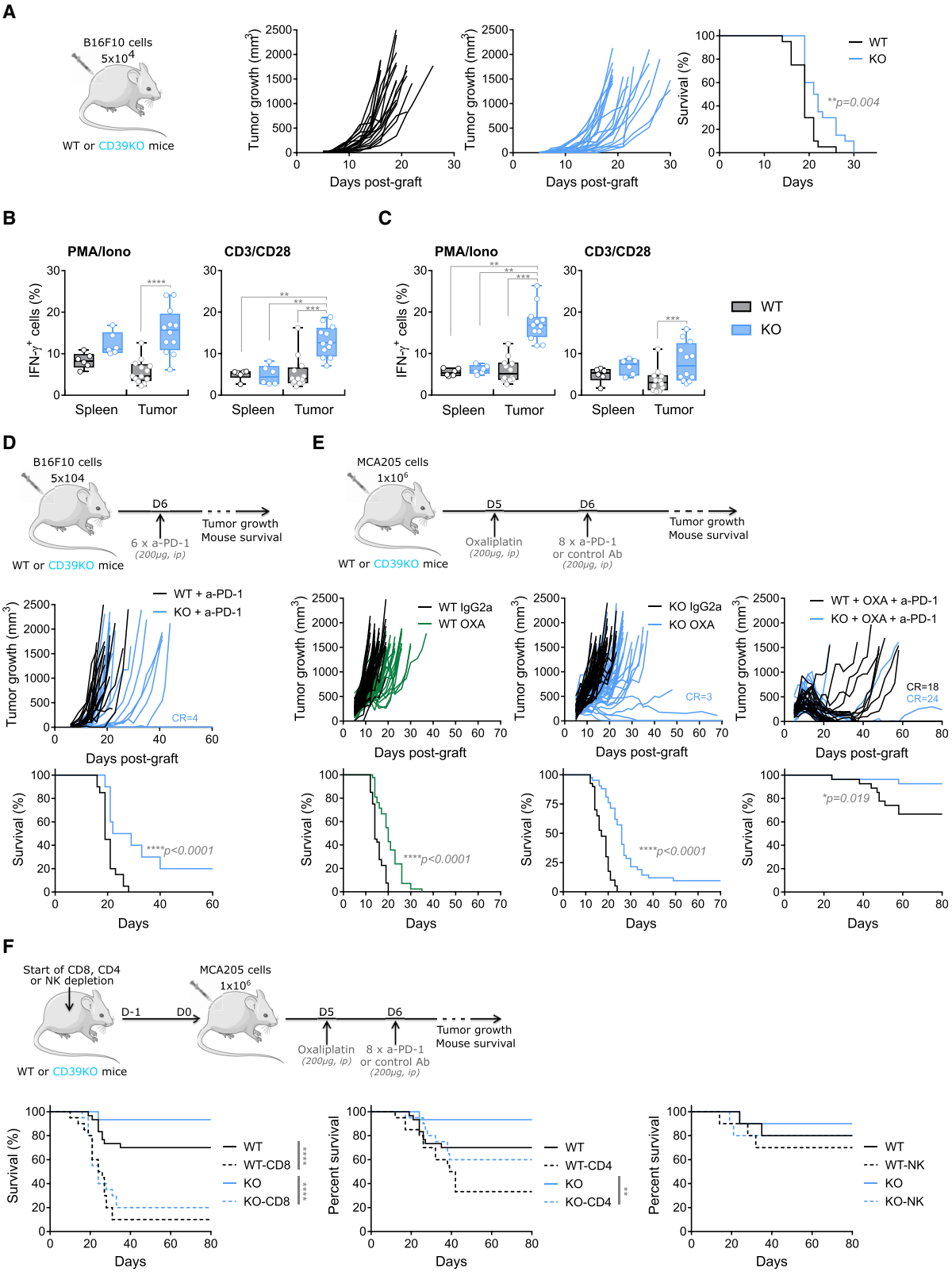

(legend on next page)

for ~90% of the CD39 expressing cells (Figure S1D, right panel). Tumor progression was also associated with increased intensity of CD39 expression on myeloid cells (not shown). Thus, the ATPase activity in the microenvironment of B16F10 tumors was provided mostly by CD39-expressing myeloid cells. The tumor infiltrate monitored in CD39-deficient animals was similar to that observed in WT mice, indicating that CD39 expression had no impact on the composition of the infiltrate (Figure S1E).

We then investigated the effects of host CD39 deficiency on the effector functions of tumor-infiltrating lymphocytes (TILs). Using splenic T cells as control, we compared the cytokine profiles after *ex vivo* stimulation of $CD8^+$ (Figure 1B) and $CD4^+$ (Figure 1C) TILs isolated from B16F10 tumors developing in WT or CD39-deficient mice. Interestingly, both $CD8^+$ and $CD4^+$ TILs from CD39-deficient mice produced more interferon (IFN)-γ than TILs from WT mice upon treatment with anti-CD3/anti-CD28 antibodies, which stimulate the T cell receptor, and after phorbol 12-myristate 13-acetate (PMA)-ionomycin stimulation, which bypasses the T cell membrane receptor complex. Thus, CD39 expression promotes tumor growth, and, conversely, its genetic deficiency promotes antitumor immunity and improves the effector activities of both $CD8^+$ and $CD4^+$ TILs.

TILs Express Both CD39 and PD-1

In the same B16F10 model, we further analyzed expression of CD39 and PD-1 exhaustion markers at the surface of the T cell populations infiltrating the tumor bed (Blank and Mackensen, 2007; Canale et al., 2018; Gupta et al., 2015a; Simoni et al., 2018). In the tumor bed, PD-1 and CD39 were expressed by both $CD8^+$ and $CD4^+$ TILs, and the frequency of CD39/PD-1 double positive infiltrating $CD8^+$ T cells was significantly increased as compared to their splenic counterparts for which the expression was barely detectable (Figure S1F, upper panels). Furthermore, the proportion of $CD39^+$ cells was higher in the exhausted PD-1-expressing $CD8^+$ TILs than in the $PD\text{-}1^-$ T cell populations (Figure S1F, lower left panel). In this model, $PD\text{-}1^+CD39^+$ double-positive TILs expressed higher levels of PD-1 and CD39 than cells positive for only CD39 (Figure S1F, lower middle panel) or PD-1 (Figure S1F, lower right panel), as previously reported (Canale et al., 2018). We extended these observations to $CD4^+$ TILs isolated from the mouse MC38 colorectal and MCA205 fibrosarcoma tumor models (data not shown). The co-expression of CD39 and PD-1 was thus a common feature of tumor-infiltrating $CD8^+$ and $CD4^+$ T cells.

We then monitored CD39 and PD-1 expression at the surface of tumors from patients, assessing the physiological relevance of our observations in mice. We first analyzed the expression of CD39 and PD-1 in human melanoma tumors by immunohistochemistry. CD39 was expressed by both immune and endothelial cells from the TME and by the tumor cells themselves (data not shown), as previously reported (Bastid et al., 2015). By contrast, PD-1 expression was restricted to immune cells (data not shown). Immunofluorescence staining of tissue sections showed that some tumor-infiltrating immune cells co-expressed CD39 and PD-1 (Figure S1G). We confirmed the presence of $CD8^+$ TILs co-expressing CD39 and PD-1 by flow cytometry on freshly dissociated stage IV melanoma tumors (Table S1). In contrast, circulating peripheral blood mononuclear cells (PBMCs) were low for these markers (Figure S1H, left panel). We confirmed these observations on another type of cancer, the squamous cell carcinoma of the head and neck (SCCHN) (Table S2). The frequencies of $CD39^+$ $PD\text{-}1^+$ T cells were higher in tumor samples from SCCHN patients than in periphery (Figure S1I, left panel). As in mouse tumor models, the frequency of $CD39^+$ cells was higher in the $PD\text{-}1^+$ than in the $PD\text{-}1^-$ subpopulation of TILs (Figures S1H and S1I, middle and left panels). We extended these observation to $CD4^+$ T cells for both cancer indications. Overall, these results point out in different tumor models the specific co-expression of CD39 and PD-1 by $CD8^+$ and $CD4^+$ T cells infiltrating the tumor bed.

CD39 Disruption Enhances Anticancer Combination Therapies

As CD39 and PD-1 were co-expressed by large numbers of TILs in mouse tumor models and on human tumor samples, we hypothesized that targeting these two distinct inhibitory pathways together would improve antitumor immunity. We tested this hypothesis by treating B16F10 melanoma-bearing WT and CD39-deficient mice with a rat IgG2a anti-PD-1 mAb (Figures 1D and S2A). The anti-PD-1 monotherapy did not affect B16F10 melanoma tumor growth in WT mice (Figure S2A). However, in CD39-deficient mice, anti-PD-1 treatment delayed tumor growth and resulted in tumor control in 20% of tumor-bearing mice, which remained tumor free (Figure 1D). Similar results were obtained with the anti-CTLA-4 mAb treatment, with 20% of the

Figure 1. The Combination of CD39 Deficiency with Chemotherapy and ICIs Promotes Tumor Elimination

(A) B16F10 tumor cells were engrafted subcutaneously in WT (n = 16) and CD39-deficient (n = 16) mice. Effective engraftment was quantified by measuring tumor volumes, and survival was monitored. Tumor growth and survival versus time were plotted. **p < 0.01; determined by log rank (Mantel-Cox) test.

(B and C) WT and CD39-deficient mice were engrafted with B16F10 tumor cells and sacrificed when tumor volume reached 300 mm^3. The frequency of IFN-γ-producing $CD8^+$ (B) and $CD4^+$ (C) TILs was determined after *ex vivo* restimulation as indicated. n = 13 for WT and n = 12 for KO mice. The data are presented as box and whiskers. **p < 0.01, ***p < 0.001, ****p < 0.0001; non-parametric Kruskal-Wallis test followed by a Dunn's multiple comparisons test.

(D) B16F10 tumor cells were engrafted subcutaneously in WT (n = 20) and CD39-deficient (n = 20) mice. Tumor-bearing mice were then treated twice weekly, from day 6, for 3 weeks, with anti-PD-1 antibody. Graphs show tumor growth in each individual and combined survival curves. CR, complete regressions.

(E) MCA205 fibrosarcoma cells were engrafted subcutaneously into WT and CD39-deficient mice. Tumor-bearing mice were then treated once with oxaliplatin (OXA) at day 5 (left panels, WT mice: green curves, n = 42; CD39-deficient mice: blue curves, n = 42) and twice weekly, from day 6, for 3 weeks with control IgG2a mAb (middle panels, WT mice: black curves, n = 40; CD39-deficient mice: blue curves, n = 40) or with anti-PD-1 antibody (right panels, WT mice: black curves, n = 27; CD39-deficient: blue curves, n = 27). Graphs show tumor growth in each individual (upper panels) and combined survival curves (lower panels).

(F) Experiment similar to that in (E) in mice receiving antibodies depleting CD8, CD4, or NK cells. Combined survival curves for n = 10 mice/group. The data presented are the pooled results of two (A and B), four (E), and three (F) independent experiments.

In (A) and (D)–(F), *p < 0.05, **p < 0.01, ****p < 0.0001; log rank (Mantel-Cox) test for Kaplan-Meier survival curves.

B16F10-engrafted CD39-deficient mice cured by treatment, whereas only 5% of WT mice survived (Figure S2B). Thus, cancer treatments with ICIs were more potent when the CD39-related Ado pathway was silenced.

We further investigated the role of CD39 in the MCA205 fibrosarcoma model to challenge our findings obtained with B16F10 melanoma cells. CD39 deficiency had little effect on the control of MCA205 tumor growth (Figure S2C). Similarly, anti-PD-1 mAb treatment in WT mice had weak effect on tumor progression (Figure S2D, upper panel). In contrast to the B16F10 mouse melanoma model, treatment with anti-PD-1 mAb in CD39-deficient mice did not lead to tumor clearance, but tumor growth was delayed (over the treatment period) in only a few anti-PD-1 mAb-treated CD39-deficient mice (Figure S2D, lower panel). We therefore sought to strengthen the immune response by combining our approaches with oxaliplatin (OXA) treatment, an immunogenic chemotherapy known to induce the release of extracellular ATP (Kroemer et al., 2013). A single injection of OXA in WT mice slightly improved tumor growth control and mouse survival following the injection of MCA205 tumor cells (Figure 1E, left panel). Tumor growth was delayed further in tumor-bearing CD39-deficient mice treated with OXA, and only a few mice could be cured (Figure 1E, middle panel). The combination of OXA and anti-PD-1 mAb treatments in WT mice improved tumor growth control, and complete tumor regressions were observed in more than 65% of tumor-bearing mice. The combination of OXA and anti-PD-1 mAb treatments in CD39-deficient mice significantly improved treatments and cured almost all the tumor-bearing mice, with close to 90% of the mice surviving the grafting of MCA205 tumors (Figure 1E, right panel). The combination therapy acted principally through $CD8^+$ T cells, with the help of $CD4^+$ T cells but not NK cells, as the injection of depleting anti-CD8β and anti-CD4 mAbs impaired survival, whereas antibodies directed against NK1.1 did not (Figure 1F). Tumor-bearing WT and CD39-deficent mice cured by combination therapies developed a long-term anti-tumor immune memory, as demonstrated by tumor re-challenge experiments (data not shown). Thus, CD39 deficiency increased the efficacy of combined ICIs and chemotherapy treatments, providing the rationale to evaluate whether the blockade of CD39 would increase treatment efficacy in cancer patients.

IPH5201 Antibody Blocks the Activities of Both Membrane-Bound and Soluble CD39

We generated anti-human CD39 antibodies and assessed their ability to block ATPase activity. We identified an anti-human CD39 mAb, IPH5201, which specifically recognized recombinant human CD39 (ENTPD1) and not CD39L1 (ENTPD2), CD39L2 (ENTPD6), CD39L3 (ENTPD3), or CD39L4 (ENTPD5) (Figure S3A). IPH5201 and the previously described BY40 had similar affinities for CD39, as shown by flow cytometry (Figure S3B) and surface plasmon resonance (SPR; Figure S3C) analyses. Neither IPH5201 nor BY40 downregulated membrane-associated CD39 (Figure S3D).

We further assessed the ectonucleotidase-blocking activity of IPH5201 relative to that of BY40. WIL2-NS and Mino CD39-expressing tumor cells (Figure S3E) were incubated with ATP in the presence or absence of the two anti-CD39 mAbs, and residual ATP levels in the supernatant were determined (Figures 2A and S3F, respectively). Both model cell lines efficiently hydrolyzed extracellular ATP, since no to low residual ATP could be detected in the absence of mAb or in the presence of an isotype control. By contrast, we observed a dose-dependent inhibition of ATP hydrolysis when cells were incubated with IPH5201. ATP hydrolysis was also decreased by the addition of BY40 mAb to the culture medium but to a lesser extent than with IPH5201 (Figures 2A and S2F). We also evaluated the efficacy of IPH5201 for blocking the soluble form of CD39 protein. Interestingly, IPH5201 efficiently blocked the enzyme activity of the soluble CD39 protein present in the supernatant of WIL2-NS and Mino cell lines, whereas BY40 did not (Figures 2B and S3G). We confirmed the ability of IPH5201, but not of BY40, to block CD39 enzyme activity on soluble recombinant CD39 protein (Figure 2C). Importantly, IPH5201 also blocked the CD39 enzymatic activity from primary tumor biopsies of melanoma, sarcoma, and ovarian cancer patients (Figure 2D; Table S3). Thus, IPH5201 anti-CD39 mAb blocked the ATPase activity of CD39 more effectively than BY40 by inhibiting both membrane and soluble forms of the enzyme.

Blocking CD39 Ectonucleotidase Activity Preserves Immunogenic ATP and Limits Immunosuppressive Adenosine Production

We hypothesized that the inhibition of ATP hydrolysis, leading to ATP accumulation, would favor the maturation and activation of DCs, as suggested in a previous study (Kroemer et al., 2013). We therefore treated monocyte-derived DCs (MoDCs) with a dose-range of ATP in the presence or not of IPH5201, BY40, or a control mAb and assessed phenotypic changes and the stimulatory potential of conditioned MoDCs. The expression of HLA-DR and CD83 were increased by ATP in presence of IPH5201 but not BY40 or control mAb (Figure 2E, middle panels). The phenotypic maturation of MoDCs observed in the presence of IPH5201 was also functionally associated with improvement in the stimulation of allogeneic CD4 T cells in a mixed lymphocyte reaction assay (Figure 2E, right panel). Finally, we evaluated the effect of CD39 blockade on the inflammasome pathway by assessing interleukin 1β (IL-1β) secretion from *in vitro*-derived M1 macrophages stimulated with lipopolysaccharide (LPS). IPH5201 efficiently promoted LPS-induced IL-1β production, whereas BY40 did not (Figure 2F, right panel). As hypothesized, IPH5201 enhanced the phenotypic maturation and the activation of DCs and macrophages by inhibiting ATP hydrolysis.

We then investigated the efficacy of IPH5201 anti-CD39 mAb for preventing the immunosuppressive effects of Ado. The proliferation of $CD4^+$ and $CD8^+$ T cell preparations enriched from human peripheral blood was strongly impaired after anti-CD3/CD28 stimulation if ATP was added to the assay. IPH5201 efficiently restored T cell proliferation in a dose-dependent manner to the levels observed in the absence of ATP addition, whereas BY40 was much less effective in restoring T cell proliferation (Figure 2G).

Thus, the blocking anti-CD39 mAb IPH5201 preserved extracellular ATP, thereby promoting the activation of DCs and

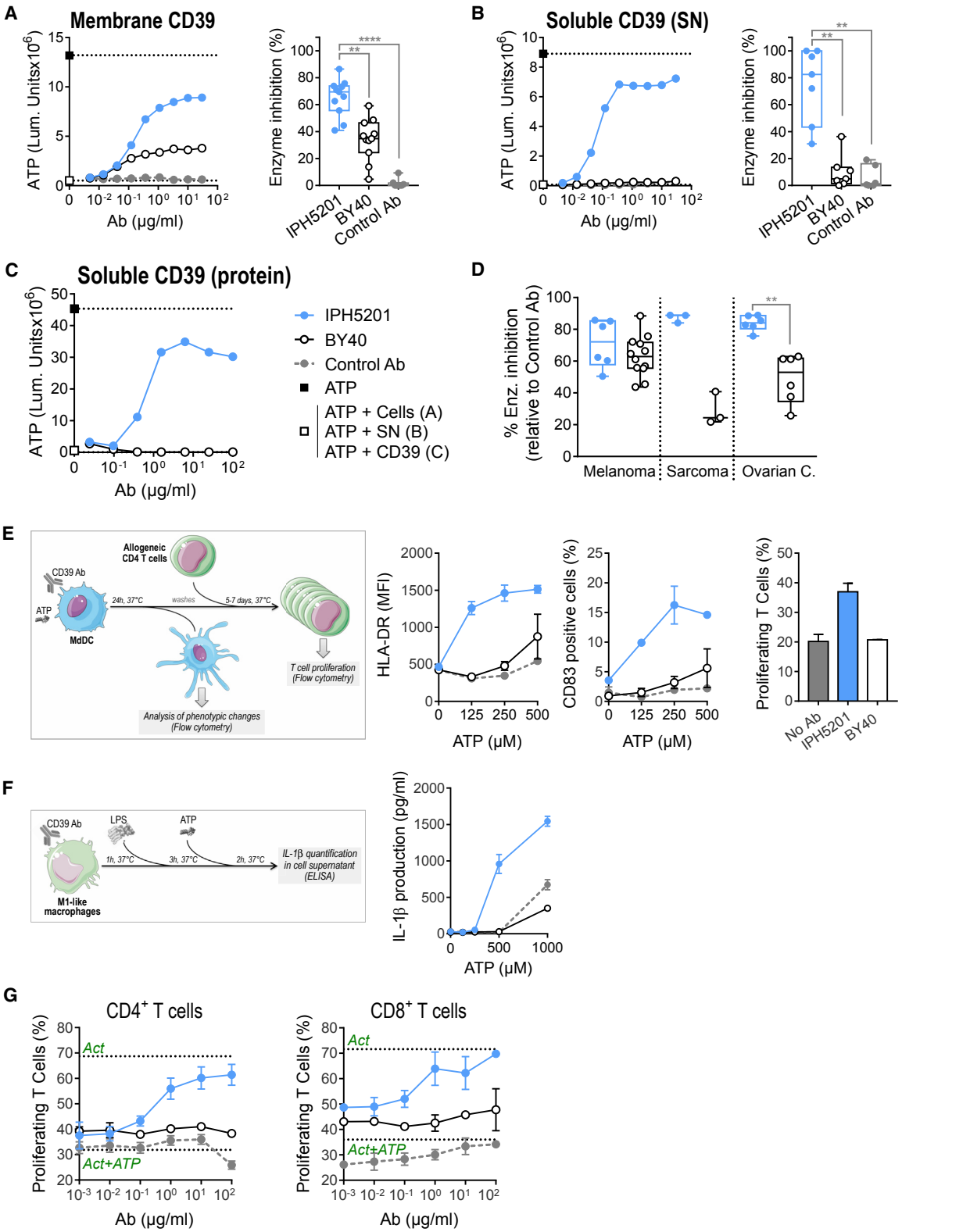

(legend on next page)

macrophages and limiting Ado accumulation and its immunosuppressive effect on T cells.

IPH5201 Blocks CD39 in Human CD39 Preclinical Mouse Model and Promotes Antitumor Immunity

We generated human CD39 knockin mice by replacing the mouse CD39 with human CD39 protein using a KO/knockin (KI) molecular biology strategy. In this model, the human CD39 expression phenocopied the expression of mouse CD39 (Figure S5A). *Ex vivo*, splenocytes from human CD39 KI mice left untreated or treated with a control mAb hydrolyzed extracellular ATP as well as cells from WT mice (Figure 3A, left panel). Murinized IPH5201 (IPH5201 with a mouse Fc silent IgG1 isotype, referred to as moIPH5201 thereafter) mouse treatment prevented *ex vivo* ATP hydrolysis by human CD39 KI cells, and ATP levels were similar to those measured for CD39-deficient cells. Similar results were obtained with spleen dissociation supernatants (Figure 3A, right panel). We further showed that *in vivo* moIPH5201 did not deplete or modify the relative number of the immune cell subsets, including CD39-expressing cells such as Treg or myeloid cells (Figure S5B). Collectively, these results showed that moIPH5201 mice treatment efficiently inhibits membrane and soluble human CD39 enzyme expressed by human CD39 KI primary immune mouse cells *ex vivo* without mediating CD39-expressing immune cell depletion *in vivo*.

We then assessed the antitumor potency of moIPH5201 in preclinical human CD39 KI mouse model grafted with MCA205 tumors (Figure 3B). As observed in CD39-deficient mice, moIPH5201 did not rescue mice from death when used as a single agent when compared to control group. By contrast, with sub-optimal regimen, chemotherapy rescued around 30% of tumor-bearing mice from death, as shown by comparison with untreated mice. A combination of IPH5201 and OXA had a synergistic effect, improving the control of tumor growth and rescuing close to 60% of the mice from death (Figure 3B). These results confirmed our previous findings showing that the blockade of the adenosinergic pathway, either by the genetic deletion of CD39 or by its blockade with moIPH5201, combined with immunogenic chemotherapy had therapeutic anti-tumor effects in preclinical mouse model.

Targeting the CD73 Enzyme Limits Immunosuppressive Adenosine Production

CD73 degrades AMP into immunosuppressive Ado. Given the potential *in vivo* redundancy of CD39 with AMP-generating enzymes such as CD38 molecule, targeting CD73 in addition to CD39 would further limit the Ado production. We thus decided to generate monoclonal antibodies blocking human CD73 enzymatic activity to complete our strategy of inhibition of the Ado pathway in patients. We selected an anti-human CD73 mAb, IPH5301. We then compared IPH5301 with two benchmarked mAbs, MEDI9447 (MedImmune) and CD73.4 (Bristol-Myers Squibb). These three mAbs had similar affinities for A375 and MDA-MB-231 CD73-expressing tumor cell lines, with similar half maximal effective concentration (EC_{50}) values (Figure S5A). SPR analysis showed that intact IPH5301 mAb and IPH5301 Fab had a K_D on recombinant CD73 similar to that of benchmarked mAbs and Fabs, respectively (Figure S5B).

We further evaluated the ability of IPH5301 to block membrane-associated and soluble CD73 enzyme activity. IPH5301 strongly inhibited AMP hydrolysis at the membrane of A375 (Figure 4A) and MDA-MB-231 (Figure S5C) cancer cells and did so more effectively than MEDI9447 and CD73.4 benchmarked mAbs. IPH5301 also blocked the activity of the soluble CD73 enzyme more effectively than the other two anti-CD73 mAbs, especially at high Ab concentration (Figures 4B and S5D). Finally, unlike MEDI9447 and CD73.4, IPH5301 did not downregulate CD73 levels at the membrane of A375 (Figure 4C) and MDA-MB-231 (Figure S5E) cell lines.

We assessed the ability of IPH5301 to reverse the immunosuppressive effect of AMP on T cells. Exogenous AMP strongly inhibited both $CD4^+$ and $CD8^+$ T cell proliferation (Figure 4D, open versus closed squares). IPH5301 blocked this inhibition in a dose-dependent manner and appeared to be more efficient than the other two anti-CD73 mAbs with both subsets

Figure 2. IPH5201 Efficiently Blocks CD39 Enzyme Activity and Promotes the Activation of T Cells, DCs, and Macrophages in the Presence of ATP

(A–C) The WIL2-NS human B cell line (A), WIL2-NS cell supernatant (B), or recombinant human CD39 protein (C) was incubated with ATP (open square) in the presence or absence of anti-CD39 IPH5201 or BY40 mAbs or control mAb over a range of doses or at a saturating dose (10 μg/ml). ATP was incubated in TBS buffer (A and C) or in culture medium (B) with no source of CD39 as a control (closed square). After 1 h (A), 2 h (B), or 30 min (C), the remaining ATP was quantified in the cell supernatant. Percentage of CD39 inhibition was plotted as the pooled results of 11 and 7 independent experiments for membrane and soluble CD39, respectively. Non-parametric Kruskal-Wallis test followed by a Dunn's multiple comparisons test. Data with recombinant human CD39 protein are representative of four experiments.

(D) Cells isolated from melanoma, sarcoma, and ovarian tumors were incubated with ATP in the presence of anti-CD39 IPH5201 or BY40 mAbs or control mAb at saturating dose (10 μg/ml). After 30 min AMP generated was quantified in cell supernatant. Percentages of inhibition of AMP generation by IPH5201 and BY40 mAbs relative to control mAb as the pooled results of 6, 1, and 2 experiments with melanoma, sarcoma, and ovarian tumors, respectively, are indicated. Regarding ovarian samples, results were obtained from two biopsies of the same patient (see STAR Methods section). Non-parametric Mann-Whitney test; $^{**}p < 0.01$.

(E) Monocytes were allowed to differentiate into dendritic cells (MoDCs), which were then incubated with anti-CD39 or control mAbs and stimulated with a range of ATP doses. The expression of HLA-DR and CD83 was assessed by flow cytometry. Median fluorescence of HLA-DR-positive cells and percentage of cells expressing CD83 are shown according to ATP dose (E, middle panels). ATP-stimulated MoDCs were extensively washed and cultured with allogeneic $CD4^+$ T cells. T cell proliferation was measured (E, right panel).

(F) Monocytes were allowed to differentiate into M1-like macrophages and were then incubated with a fixed dose of anti-CD39 or control mAbs and stimulated with LPS and then with a range of ATP doses. IL-1β production was determined according to the dose of ATP (F, right panel). Data are representative of four experiments in (E) and (F).

(G) Human lymphocyte-enriched peripheral blood cell preparations were activated with anti-CD3/anti-CD28 antibody-coated beads in the presence of ATP and a range of doses of anti-CD39 or control mAbs. T cell proliferation was assessed by flow cytometry. Data are representative of at least 3 experiments.

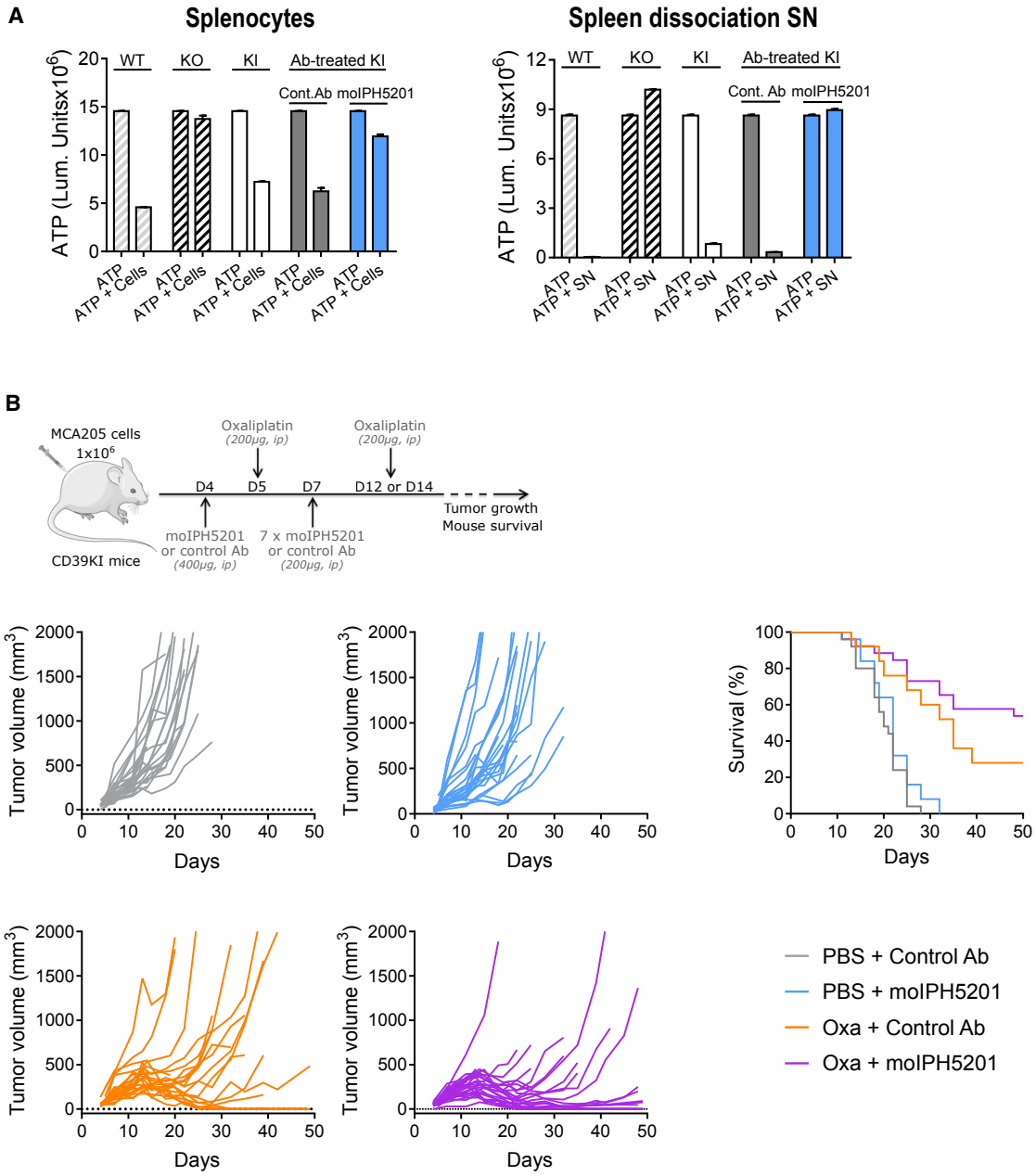

Figure 3. IPH5201 Efficiently Impairs CD39 Enzyme Activity on Splenocytes from KI Mice and Synergizes with OXA to Promote Anti-Tumor Immunity

(A) Human CD39 KI mice were injected with IPH5201 or control mAbs for 20 h before spleen collection. Isolated spleen cells (left panel) and cell dissociation supernatants (right panel) were incubated with 20 µM ATP at 37°C for 2 h and 30 min, respectively. Residual ATP was measured in the supernatant of each condition. WT and mouse CD39 KO mice were used as control. Data are presentative of 2 experiments.

(B) Anti-tumor potency of IPH5201 combined with OXA was assessed in human CD39KI mice as diagrammed. Tumor growth and mouse survival were monitored for 50 days. Results are a pool of 2 independent experiments on 13 and 12 mice per group, respectively.

(Figures 4D and 4E). We then investigated whether IPH5301 could block the Ado-mediated suppression of T cell proliferation in a MLR model (Figure 4F). MoDCs induced a potent proliferation of allogeneic T cells that was inhibited by the addition of ATP (Figure 4F, middle panel). IPH5301 blocked the ATP-mediated T cell suppression, in a dose-dependent manner (Figure 4F, right panel). Overall, these results indicate that blocking CD73 enzyme activity with IPH5301 efficiently inhibits ATP-derived AMP hydrolysis into Ado, thereby promoting T cell proliferation, with a different mechanism of action compared to benchmarked mAbs as it does not induce internalization, while being more active in several tests.

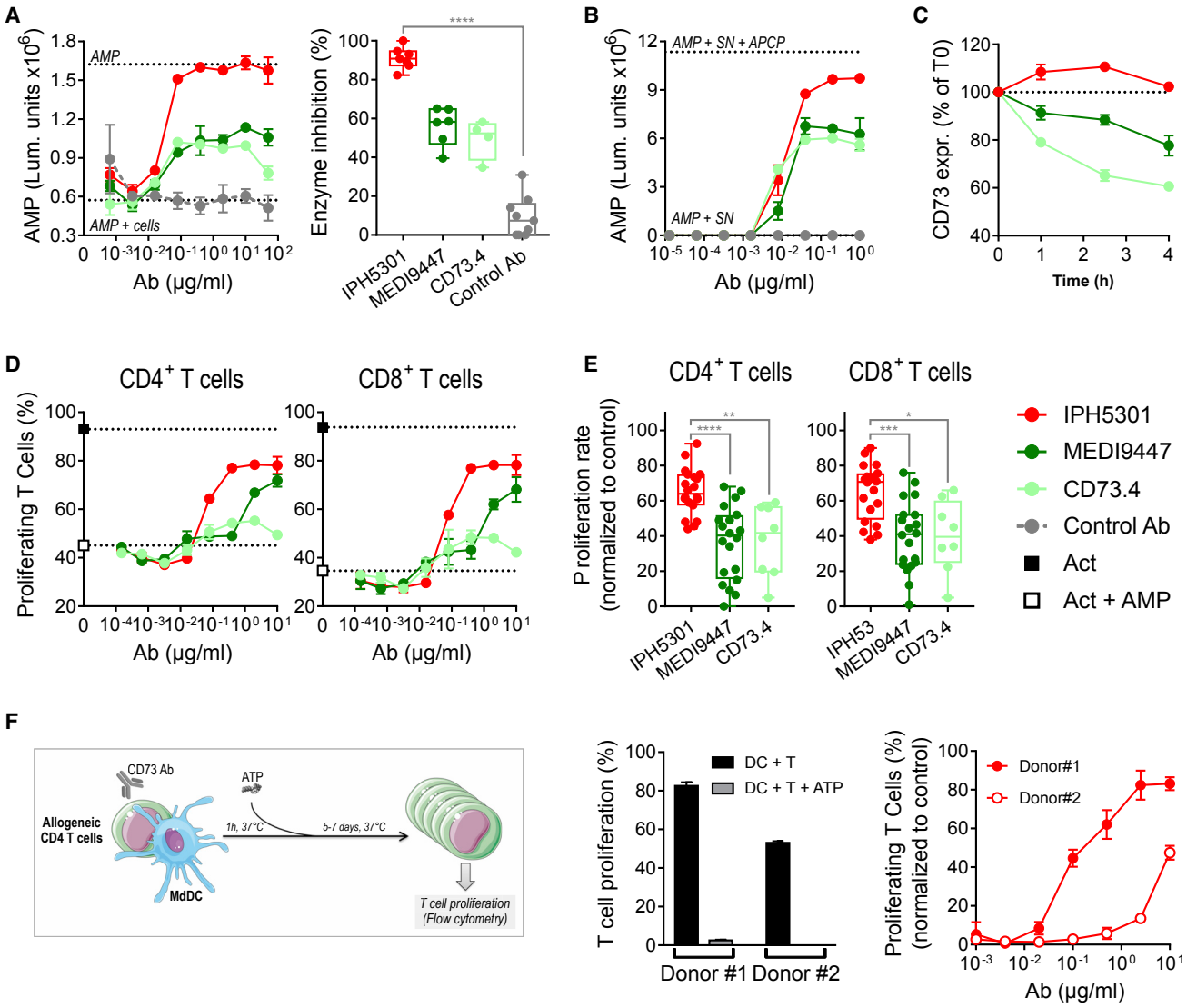

Figure 4. IPH5301 Blocks Membrane-Associated and Soluble Forms of CD73 Enzyme and Attenuates AMP-Mediated T Cell Suppression

(A and B) A375 human melanoma cells (A) or A375 cell supernatant (B) were incubated with AMP in the presence or absence of anti-CD73 (IPH5301, MEDI9447, and CD73.4) or control mAbs over a range of doses or at the saturating concentration of 10 µg/ml. After 1 h (A) or 2 h (B) of incubation, the AMP remaining in the cell supernatant was quantified. Percentage of enzyme inhibition was plotted as the pooled results of at least four experiments. Non-parametric Kruskal-Wallis test followed by a Dunn's multiple comparisons test. Data using A375 cell supernatant are representative of 4 experiments.

(C) Ability of anti-CD73 mAbs to induce CD73 downregulation was assessed by incubating A375 cells with 10 µg/ml anti-CD73 mAbs at 37°C. CD73 expression analyzed by flow cytometry was standardized relative to T0 expression and plotted against time. Data are representative of 3 experiments.

(D) Experiment similar to that in Figure 2G except that suppression was induced by AMP rather than ATP. Data are representative of at least 8 independent experiments.

(E) The maximal potency of the mAbs to reverse ATP-mediated T cell suppression was determined at a concentration of 10 µg/ml anti-CD73 or control mAbs. Data are a pool of at least eight independent experiments. Non-parametric Kruskal-Wallis test followed by a Dunn's multiple comparisons test.

(F) MoDCs were cultured with allogeneic $CD4^+$ T cells in the presence or absence of range of doses of anti-CD73 IPH5301 mAb and an immunosuppressive dose of ATP (100 µM). T cell proliferation was evaluated by flow cytometry. Percentages of T cells proliferating in the presence or absence of ATP (middle panel, two independent experiments) and in the presence of increasing doses of IPH5301 mAb (right panel) are shown.

IPH5301 Blocks Enzyme Activity by Constraining CD73 in an Intermediate Conformation

To get more insight into the mechanism of action of the IPH5301 blocking mAb, we dissected its association with CD73 using two complementary approaches. First, the negative staining of the CD73-IPH5301 complex analyzed by electron microscopy revealed that the intact IPH5301 mAb interacts with the N-terminal domains of the CD73 dimers mainly in a 1:1 stoichiometry (i.e., 1 IPH5301 mAb for 1 CD73 dimer; Figure 5A). This observation was confirmed by the electronic microscopy image of a

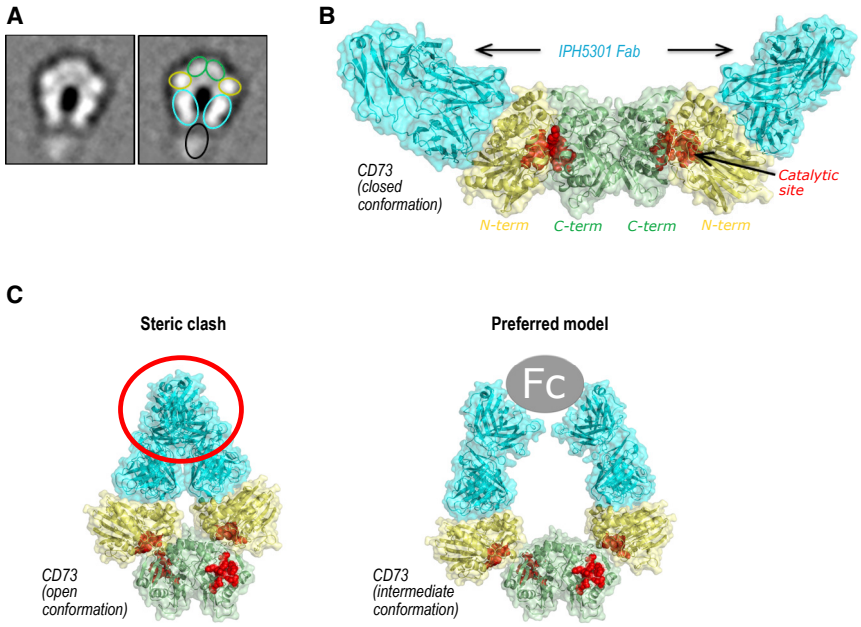

Figure 5. Crystal Structure of CD73 and IPH5301 Fab Complex

(A) Negative staining of the CD73-IPH5301 (whole Ig) complex. The right panel represents the CD73 dimer (N-terminal domain, green; C-terminal domain, yellow) and IPH5301 mAb (Fab, cyan-blue; Fc, black) on a 2D class average calculated from the recorded pictures. Presented data are representative of the main complex observed on the grid (see Figure S6C).

(B) Crystal structure of CD73 and IPH5301 Fab complex. The N- and C-terminal domains of the dimer are shown in yellow and green, respectively. The IPH5301 Fab is shown in cyan-blue. Residues involved in the catalytic site of CD73 are shown in red.

(C) Models extrapolated of the crystal structure of CD73-IPH5301 Fab complex. The left panel shows the complex in the open conformation of CD73. The right panel the complex in an intermediate conformation of CD73 (preferred model). Color codes are as in (B).

complete field of particles and a SDS-PAGE analysis of IPH5301 and CD73 ectodomain main complexes collected after gel filtration using a Superose 6 column (Figures S6A–S6C). Second, we determined the crystal structure of IPH5301 Fab in complex with the ectodomain of CD73 to 2.78 Å resolution (PDB: 6HXW). There is a zero occupancy for the constant domains (both light and heavy chains) of one IPH5301 Fab as it was not stabilized in the crystal packing. However, the variable chains of this Fab is well defined in the electron density map, indicating that it was present in the crystal (Figure S6D). Thus, we set the occupancy to zero for the corresponding atoms (816 atoms out of a total of 14,641). This analysis indicated that IPH5301 Fab interacts with the catalytically active closed state of CD73 (Figure 5B; Table S4). Indeed, previous structural studies of CD73 have shown that its enzymatic activity requires extensive N-terminal domain rotation defining open (inactive) and closed (active) states of the enzyme (Knapp et al., 2012). Taken into consideration the 1:1 stoichiometry between an intact IPH5301 mAb and a CD73 dimer, it is anticipated that steric hindrance would make it unlikely that the intact mAb could bind to CD73 open conformers (Figure 5C, left panel). Our data thus support a model for the mode of action of IPH5301, as the intact mAb constrains CD73 in an intermediate state in which AMP could not be hydrolyzed (Figure 5C, right panel). This model is further supported by the fact that monovalent IPH5301 Fab failed to block membrane-associated CD73 enzymatic activity (Figure S6E). Furthermore, the IPH5301 Fab orientation on the N-terminal domain of CD73 is compatible with an intra-dimer binding mode as it is located right on the apex of the molecule (not shown) in contrast to Medi9447 and CD73.4 mAbs, whose epitopes are eccentric and that are described to interact with CD73 in an inter-dimer mode (Geoghegan et al., 2016; Larrick et al., 2016). Finally, the absence of detectable downregulation of CD73 by IPH5301 immunoglobulin G (IgG) is consistent with intra-dimer binding, rather than the downregulation-inducing crosslinking expected from inter-dimer contacts.

The Combination of IPH5201 and IPH5301 Releases ATP-Mediated Suppression of T Cells from Healthy Donors and Cancer Patients

We have shown that TILs from cancer patients expressed a high level of CD39 and that inhibition of the immunosuppressive Ado pathway stimulated T cell proliferation. We next investigated whether the IPH5201 and IPH5301 mAbs blocked the immunosuppressive Ado pathway in PBMCs obtained from breast cancer patients. The addition of extracellular ATP to activated-PBMCs reduced $CD4^+$ and $CD8^+$ T cell proliferation (Figures 6A and 6B). Saturating doses of either anti-CD39 or anti-CD73 mAbs, used as single agents, abolished the suppression of $CD4^+$ and $CD8^+$ T cells by extracellular ATP, as shown by comparisons with control mAb (Figures 6A and 6B).

As previously mentioned, some membrane ATPase may generate AMP and mediate immunosuppression through Ado that could overcome the sole blockade of CD39. In light of these data, we investigated whether the combination of IPH5201 and IPH5301 could synergize to block the adenosinergic pathway. Dose-ranges of IPH5201 and IP5301 mAbs were used to treat PBMCs from healthy donors in combination with sub-optimal doses of IPH5301 and IPH5201, respectively. As previously observed (Figure 6B), saturating doses of both mAbs potently blocked ATP-mediated T cell suppression. When used in combination at inefficient suboptimal doses, the anti-CD39/CD73 mAbs acted in synergy to abrogate suppressive effect of ATP and promote the proliferation of T cells from healthy donors (Figures 6C and 6D). Similar results were obtained for T cells from breast cancer patient PBMCs (Figure 6E and Table S5). Overall, these data suggest that the concomitant blockade of both CD39 and CD73 immunosuppressive enzyme can limit

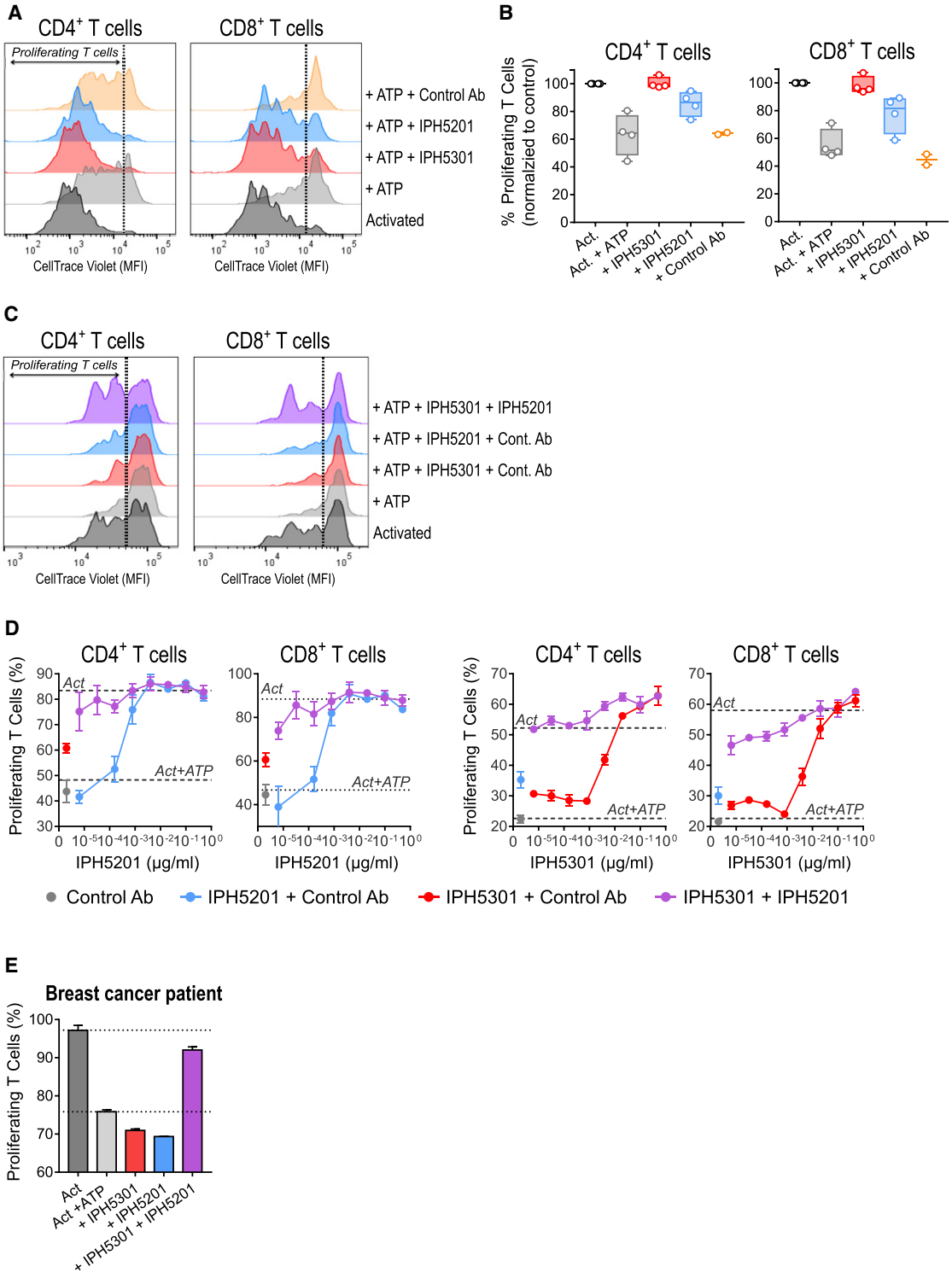

Figure 6. Combination of IPH5201 and IPH5301 to Attenuate ATP-Mediated T Cell Suppression in Cells from Healthy Donors and Cancer Patients

(A and B) PBMCs from breast cancer patients were activated with anti-CD3/anti-CD28 antibody-coated beads in the presence or absence of 500 μM ATP and 10 μg/ml IPH5201, IPH5301, or control mAbs. T cell proliferation was assessed by measuring dye dilution by flow cytometry.

(A) Fluorescence-activated cell sorting (FACS) profiles. Data are representative of four independent experiments.

(legend continued on next page)

Ado-mediated T cell inhibition, thereby enhancing anti-tumor immunity.

DISCUSSION

Primary or acquired resistance to cancer immunotherapy is common, prompting the identification of predictive markers and the causes of resistance mechanisms to ICIs (Sharma et al., 2017). An increase of CD39 and CD73 at the tumor bed signals an immunosuppressive environment inhibiting anti-tumor immune responses and favoring tumor spreading. Combining genetic and antibody-mediated approaches, we investigated here the impact of blocking CD39 and CD73 ectoenzymes to overcome Ado-mediated immunosuppression and reinforce anti-tumor immunity.

Besides its well-described ATPase activity, deep phenotypic profiling of tumor microenvironment identifies CD39-expressing T cells as a specific cell subtype of TILs (Canale et al., 2018; Gupta et al., 2015b; Simoni et al., 2018). We confirm here the co-expression of CD39 and PD-1 by TILs in melanoma, fibrosarcoma, and colon cancer preclinical mouse models as well as in human melanoma and head and neck squamous cell carcinoma (HNSCC) specimens. We used therapy-resistant mouse models or inefficacious treatment regimens to assess the capacity of CD39 blockade to modulate the immune response to chemotherapies and ICIs. We demonstrated an increased efficacy of anti-PD-1 and anti-CTLA-4 treatments in CD39-deficient animals grafted with a B16-F10 melanoma cell line. Using MCA205, a sarcoma tumor model resistant to PD-1 treatment when used as single agent, we showed that suboptimal chemotherapy regimen enhanced the effects of anti-PD-1 treatment in WT mice. These synergistic effects were improved in CD39-deficient mice as the combination of both therapies rescued almost all the mice from death. Thus, the genetic deletion of CD39 ectonucleotidase in combination with other cancer treatments is beneficial and improves anti-tumor immunity. These results reinforce the previous demonstration that blockade of Ado generation via CD73 or its signaling through A2AR act in synergy with anti-PD-1 or anti-CTLA-4 mAbs in preclinical studies (Allard et al., 2013; Beavis et al., 2013; Iannone et al., 2014; Waickman et al., 2012). Based on these data, phase I/II clinical trials evaluating the blockade of CD73 or A2AR in combination with inhibitors of the PD-1/PD-L1 axis are currently being conducted (NCT02503774, NCT03611556, NCT03616886, NCT02655822, NCT03549000, and NCT03454451).

In line with our preclinical mouse model data, we generated an anti-CD39 mAb, IPH5201, which was found to be more effective than the previously reported membrane CD39 blocking mAb, BY40, as IPH5201 inhibited both the membrane-bound and soluble forms of the enzyme. By inhibiting the degradation of ATP, IPH5201 not only limits Ado accumulation and its immunosuppressive effect on effector T cells but also efficiently promotes the activation of DCs and macrophages through the maintenance of the extracellular ATP pool. The dual effect of IPH5201 might be most interesting for the design of combinatorial therapies as the efficient release and accumulation of ATP appear to be critical for the immunogenic response after chemotherapy treatment. Indeed, chemotherapeutic agents, such as OXA and mitoxantrone that induce ATP release, fail to elicit an efficient immunogenic response in $CD39^{+}$ cancer cells, due to a CD39-dependent ATP hydrolysis (Michaud et al., 2011). In addition to the priming of the immune response, extracellular ATP is also known to specifically inhibit tumor cell proliferation and to promote cancer cell death (Feng et al., 2011; White and Burnstock, 2006). The pluripotent role of ATP in eliciting potent anti-tumor response strengthened the interest of blocking CD39 ATPase activity for the treatment of cancer. Encouragingly, we confirmed the therapeutic potential of moIPH5201 in combination with immunogenic chemotherapy, using a human CD39 KI mouse model. Altogether, these observations paved the way to clinical trials of IPH5201 mAb in cancer patients.

However, there might be conditions where other enzymes generating AMP, such as NPP1 or CD38, can compensate for the lack of CD39 activity and lead to generation of Ado in the tumor microenvironment. In this context, the blockade of the adenosinergic pathway downstream of ATP hydrolysis (i.e., CD73, Ado receptors) is of most interest. We generated an anti-CD73 mAb that inhibited both the membrane-bound and soluble forms of the enzyme more effectively than benchmark mAbs (i.e., MEDI9447 from MedImmune, BMS986179 from Bristol-Myers Squibb), with differentiated mechanism of action. Anti-CD73 mAbs are currently under evaluation in phase I/II clinical trials, either alone or in combination with durvalumab, nivolumab, or pembrolizumab and adenosine receptor (AdoR) inhibitors, tyrosine kinase inhibitors (TKIs), and chemotherapies for the treatment of advanced solid tumors. Preliminary data for the combinations indicate a tolerable safety profile similar to those for durvalumab or nivolumab monotherapies, consistent with minor phenotypic modification observed in KO mice (Blume et al., 2012; Sun et al., 2010). Furthermore, promising anti-tumor efficacy was observed with both anti-CD73 mAbs in combination with PD-(L)1 blockers, reinforcing the interest of blocking CD73 in combination with ICIs (Siu et al., 2018; Overman et al.,

(B) The percentage of T cells proliferating is shown. Results are normalized relative to the corresponding maximal proliferation conditions obtained without ATP for each patient. T cell proliferation was plotted as the pooled results of four different patients.
(C and D) PBMCs from healthy donors were activated with anti-CD3/anti-CD28 antibody-coated beads in the presence or absence of 500 μM ATP and of the indicated doses of IPH5201, IPH5301, or control mAbs. T cell proliferation was assessed as described previously.
(C) FACS profiles. Data are representative of 5 experiments with independent donors.
(D) The percentage proliferation of T cells is shown. The upper panel shows dose range of IPH5301 alone (red curve) or in combination with 1 μg/ml of IPH5201 (purple curve). Potency of IPH5201 at 1 μg/ml is also shown (blue symbol). The lower panel shows dose range of IPH5201 alone (blue curve) or in combination with 10^{-3} μg/ml of IPH5301 (purple curve). Potency of IPH5201 at 10^{-3} μg/ml is also shown (red symbol). Data are representative of at least five experiments with independent donors.
(E) Experiment similar to that in (C) and (D) with PBMCs from breast cancer patients. Presented IPH5201 and IPH5301 concentrations (alone or in combination) are 10^{-1} μg/ml and 10^{-2} μg/ml, respectively. Data are representative of three experiments performed on independent human subjects.

2018). The development of IPH5301 for clinic al use in several human cancer indications is therefore underway.

Besides the combination of inhibitors of the adenosinergic pathway with conventional or targeted therapies and immune checkpoint blockers, it remains to be addressed whether co-blockade of CD39, CD73, and/or A2AR might be redundant or not. Interestingly, the co-inhibition of CD73 and A2AR has been shown to improve anti-tumor immune responses and limit tumor initiation, growth, and metastasis in breast, melanoma, and fibrosarcoma preclinical models (Young et al., 2016). Furthermore, recent data showed that human tumor cells may express CD38, an ectoenzyme that mediated immunosuppression through the indirect production of AMP, thus of Ado, and favored tumor cell escape from PD-1/PD-L1 axis blockade (Chen et al., 2018). In this context, we anticipated a synergistic effect of CD39 and CD73 blocking antibodies to improve anti-tumor immune responses. A differentiated effect of blocking CD39, contrary to A2AR or CD73 inhibitors, is to preserve the immunostimulatory ATP pool. Indeed, by limiting the generation of Ado, a major inhibitor of effector T cell and NK cell antitumor activities, and increasing levels of extracellular ATP, an inhibitor of tumor cell proliferation and an essential sensor molecule that attracts antigen-presenting cells to the tumor site, we expected a clinical benefit of the association. As a first step, we demonstrated here that both IPH5201 and IPH5301 mAbs efficiently block ATP-mediated inhibition of activated T cells. More importantly, when used at sub-optimal concentrations, both antibodies act in synergy to restore proliferation of T cells within PBMC obtained from healthy donors and breast cancer patients.

In conclusion, we report here the positive impact of blocking the CD39 and the CD73 ectoenzymes on the immune system and the generation of two mAbs, IPH5201 and IPH5301, targeting the CD39 and CD73, respectively. These mAbs inhibited the Ado pathway more effectively than the previously described mAbs. The clinical development of IPH5201 and IPH5301 should be beneficial for several human cancer indications, particularly if these mAbs are used in combination with each other, with ICIs, and with chemotherapies.

STAR★METHODS

Detailed methods are provided in the online version of this paper and include the following:

- KEY RESOURCES TABLE
- CONTACT FOR REAGENT AND RESOURCE SHARING
- EXPERIMENTAL MODEL AND SUBJECT DETAILS
  - Human Subjects
  - Mice
  - Cell lines
- METHOD DETAILS
  - Antibody cloning, chimerization and purification
  - Flow cytometry
  - Murine tumor models and treatments
  - AMP determination by MALDI-TOF spectrometry
  - Isolation of immune cells
  - Blockade of membrane-associated CD39 or CD73 activity
  - Blockade of soluble CD39 or CD73 activity
  - *In vitro* enzymatic assay on recombinant soluble CD39
  - T cell proliferation assay
  - Allogeneic mixed Lymphocyte Reaction (MLR) assay
  - CD39 effect on inflammasome pathway
  - Protein expression and purification for crystallization study
  - Negative Staining of CD73-IPH5301 complex
  - Crystallization, data collection and processing
  - Structure determination
  - ELISA to assess recognition of CD39 and CD39-like proteins
  - SPR analysis to assess Ab KD on recombinant CD39 or CD73 proteins
- QUANTIFICATION AND STATISTICAL ANALYSIS
- DATA AND SOFTWARE AVAILABILITY

SUPPLEMENTAL INFORMATION

Supplemental Information can be found online at https://doi.org/10.1016/j.celrep.2019.04.091.

ACKNOWLEDGMENTS

We thank the CRB-ICM (BB-033-0059) and CRB-CHUM (BB-033-00031) for supplying biological resources; M. Blemont, C. Denis, A. Morel, C. Soulas, C. Bonnafous, G. Alberici, F. Boissière-Michot, and J. Simony-Lafontaine for their expertise and advice; B. Guillot and P.-E. Colombo for providing tumor specimens; and A. Lalanne and O. Lantz for flow cytometry analyses on head and neck cancer samples. This work was supported by the European Community's Seventh Framework Program, the French Infrastructure for Integrated Structural Biology (FRISBI), Agence Nationale pour la Recherche, Cancéropole Grand Sud-Ouest, the French National Research Agency under the program "Investissements d'avenir" grant agreement LabEx MAbImprove, FRM, and Fondation pour la recherche Nuovo Soldati. The E.V. lab is supported by funding from the European Research Council (ERC) under the European Union's Horizon 2020 research and innovation programme (TILC, grant agreement 694502); the Agence Nationale de la Recherche; Equipe Labellisée "La Ligue," Ligue Nationale contre le Cancer; MSDAvenir; Innate Pharma; and institutional grants to the CIML (INSERM, CNRS, and Aix-Marseille University) and to Marseille Immunopôle. MI-mAbs (F.R.) is partially funded by an ANR grant from "Investissement d'avenir, preindustrial demonstrator."

AUTHOR CONTRIBUTIONS

I.P., H.-A.M., M.G.-P., S.A., L. Gros, C.D., A.D., R.C., D.J., H.R.-B., B.R., S.C., N.G., and O.B. performed and analyzed the experiments. O.B. helped with patient recruitment, obtaining consent, and sample collection. A.B., J.-F.E., and J.B. initiated the CD39 research program and contributed to project development. FR lab (MI-mAbs) generated CD39 and CD73 antibodies and participated in their characterization. L. Gauthier designed humanized variants for IPH5201 and IPH5301. B.A. and A.R. resolved co-crystals of CD73 and IPH5301 Fab. I.P., Y.M., C.P., and N.B. supervised the study. I.P., H.-A.M., E.N.-M., C.P., N.B., and E.V. wrote the manuscript with the help of all co-authors.

DECLARATION OF INTERESTS

I.P., M.G.-P., S.A., R.C., D.J., H.R.-B., L. Gauthier, B.R., S.C., N.G., Y.M., E.V., and C.P. are employees and shareholders of Innate Pharma. A.D., C.D., and J.B. are employees of OREGA Biotech. A.B., J.-F.E., N.B., and J.B. are shareholders of OREGA Biotech. I.P., L. Gauthier, B.R., S.C., Y.M., and C.P. hold patents related to anti-CD39 antibodies and anti-CD73 antibodies. J.B.,

A.B., J.-F.E., and N.B. hold patents related to anti-CD39 antibodies. The other authors declare no conflict of interest.

Received: October 18, 2018
Revised: December 26, 2018
Accepted: April 18, 2019
Published: May 21, 2019

REFERENCES

Allard, B., Pommey, S., Smyth, M.J., and Stagg, J. (2013). Targeting CD73 enhances the antitumor activity of anti-PD-1 and anti-CTLA-4 mAbs. Clin. Cancer Res. *19*, 5626–5635.

Allard, B., Turcotte, M., Spring, K., Pommey, S., Royal, I., and Stagg, J. (2014). Anti-CD73 therapy impairs tumor angiogenesis. Int. J. Cancer *134*, 1466–1473.

Antonioli, L., Yegutkin, G.G., Pacher, P., Blandizzi, C., and Haskó, G. (2016). Anti-CD73 in cancer immunotherapy: awakening new opportunities. Trends Cancer *2*, 95–109.

Antonioli, L., Novitskiy, S.V., Sachsenmeier, K.F., Fornai, M., Blandizzi, C., and Haskó, G. (2017). Switching off CD73: a way to boost the activity of conventional and targeted antineoplastic therapies. Drug Discov. Today *22*, 1686–1696.

Bastid, J., Regairaz, A., Bonnefoy, N., Déjou, C., Giustiniani, J., Laheurte, C., Cochaud, S., Laprevotte, E., Funck-Brentano, E., Hemon, P., et al. (2015). Inhibition of CD39 enzymatic function at the surface of tumor cells alleviates their immunosuppressive activity. Cancer Immunol. Res. *3*, 254–265.

Beavis, P.A., Divisekera, U., Paget, C., Chow, M.T., John, L.B., Devaud, C., Dwyer, K., Stagg, J., Smyth, M.J., and Darcy, P.K. (2013). Blockade of A2A receptors potently suppresses the metastasis of CD73+ tumors. Proc. Natl. Acad. Sci. USA *110*, 14711–14716.

Blanc, E., Roversi, P., Vonrhein, C., Flensburg, C., Lea, S.M., and Bricogne, G. (2004). Refinement of severely incomplete structures with maximum likelihood in BUSTER-TNT. Acta Crystallogr. D Biol. Crystallogr. *60*, 2210–2221.

Blank, C., and Mackensen, A. (2007). Contribution of the PD-L1/PD-1 pathway to T-cell exhaustion: an update on implications for chronic infections and tumor evasion. Cancer Immunol. Immunother. *56*, 739–745.

Blume, C., Felix, A., Shushakova, N., Gueler, F., Falk, C.S., Haller, H., and Schrader, J. (2012). Autoimmunity in CD73/Ecto-5′-nucleotidase deficient mice induces renal injury. PLoS ONE *7*, e37100.

Canale, F.P., Ramello, M.C., Núñez, N., Araujo Furlan, C.L., Bossio, S.N., Gorosito Serrán, M., Tosello Boari, J., Del Castillo, A., Ledesma, M., Sedlik, C., et al. (2018). CD39 Expression Defines Cell Exhaustion in Tumor-Infiltrating $CD8^+$ T Cells. Cancer Res. *78*, 115–128.

Chen, L., Diao, L., Yang, Y., Yi, X., Rodriguez, B.L., Li, Y., Villalobos, P.A., Cascone, T., Liu, X., Tan, L., et al. (2018). CD38-Mediated Immunosuppression as a Mechanism of Tumor Cell Escape from PD-1/PD-L1 Blockade. Cancer Discov. *8*, 1156–1175.

Chen, V.B., Arendall, W.B., 3rd, Headd, J.J., Keedy, D.A., Immormino, R.M., Kapral, G.J., Murray, L.W., Richardson, J.S., and Richardson, D.C. (2010). MolProbity: all-atom structure validation for macromolecular crystallography. Acta. Crystallogr. D. Biol. Crystallogr. *66*, 12–21.

de Andrade Mello, P., Coutinho-Silva, R., and Savio, L.E.B. (2017). Multifaceted Effects of Extracellular Adenosine Triphosphate and Adenosine in the Tumor-Host Interaction and Therapeutic Perspectives. Front. Immunol. *8*, 1526.

Emsley, P., and Cowtan, K. (2004). Coot: model-building tools for molecular graphics. Acta. Crystallogr. D. Biol. Crystallogr. *60*, 2126–2132.

Emsley, P., Lohkamp, B., Scott, W.G., and Cowtan, K. (2010). Features and development of Coot. Acta Crystallogr. D Biol. Crystallogr. *66*, 486–501.

Evans, P. (2006). Scaling and assessment of data quality. Acta Crystallogr. D Biol. Crystallogr. *62*, 72–82.

Feng, L., Sun, X., Csizmadia, E., Han, L., Bian, S., Murakami, T., Wang, X., Robson, S.C., and Wu, Y. (2011). Vascular CD39/ENTPD1 directly promotes tumor cell growth by scavenging extracellular adenosine triphosphate. Neoplasia *13*, 206–216.

Geoghegan, J.C., Diedrich, G., Lu, X., Rosenthal, K., Sachsenmeier, K.F., Wu, H., Dall'Acqua, W.F., and Damschroder, M.M. (2016). Inhibition of CD73 AMP hydrolysis by a therapeutic antibody with a dual, non-competitive mechanism of action. MAbs *8*, 454–467.

Gupta, P.K., Godec, J., Wolski, D., Adland, E., Yates, K., Pauken, K.E., Cosgrove, C., Ledderose, C., Junger, W.G., Robson, S.C., et al. (2015a). CD39 Expression Identifies Terminally Exhausted CD8+ T Cells. PLoS Pathog. *11*, e1005177.

Gupta, P.K., Jaiswal, A.K., Asthana, S., Dube, A., and Mishra, P.R. (2015b). Antigen presenting cells targeting and stimulation potential of lipoteichoic acid functionalized lipo-polymerosome: a chemo-immunotherapeutic approach against intracellular infectious disease. Biomacromolecules *16*, 1073–1087.

Häusler, S.F., Del Barrio, I.M., Diessner, J., Stein, R.G., Strohschein, J., Hönig, A., Dietl, J., and Wischhusen, J. (2014). Anti-CD39 and anti-CD73 antibodies A1 and 7G2 improve targeted therapy in ovarian cancer by blocking adenosine-dependent immune evasion. Am. J. Transl. Res. *6*, 129–139.

Hayes, G.M., Cairns, B., Levashova, Z., Chinn, L., Perez, M., Theunissen, J.W., Liao-Chan, S., Bermudez, A., Flory, M.R., Schweighofer, K.J., and H van der Horst, E. (2015). CD39 is a promising therapeutic antibody target for the treatment of soft tissue sarcoma. Am. J. Transl. Res. *7*, 1181–1188.

Hilchey, S.P., Kobie, J.J., Cochran, M.R., Secor-Socha, S., Wang, J.C., Hyrien, O., Burack, W.R., Mosmann, T.R., Quataert, S.A., and Bernstein, S.H. (2009). Human follicular lymphoma CD39+-infiltrating T cells contribute to adenosine-mediated T cell hyporesponsiveness. J. Immunol. *183*, 6157–6166.

Iannone, R., Miele, L., Maiolino, P., Pinto, A., and Morello, S. (2014). Adenosine limits the therapeutic effectiveness of anti-CTLA4 mAb in a mouse melanoma model. Am. J. Cancer Res. *4*, 172–181.

Jackson, S.W., Hoshi, T., Wu, Y., Sun, X., Enjyoji, K., Cszimadia, E., Sundberg, C., and Robson, S.C. (2007). Disordered purinergic signaling inhibits pathological angiogenesis in cd39/Entpd1-null mice. Am. J. Pathol. *171*, 1395–1404.

Kabsch, W. (2010). Xds. Acta. Crystallogr. D. Biol. Crystallogr. *66*, 125–132.

Knapp, K., Zebisch, M., Pippel, J., El-Tayeb, A., Müller, C.E., and Sträter, N. (2012). Crystal structure of the human ecto-5′-nucleotidase (CD73): insights into the regulation of purinergic signaling. Structure *20*, 2161–2173.

Kroemer, G., Galluzzi, L., Kepp, O., and Zitvogel, L. (2013). Immunogenic cell death in cancer therapy. Annu. Rev. Immunol. *31*, 51–72.

Künzli, B.M., Bernlochner, M.I., Rath, S., Käser, S., Csizmadia, E., Enjyoji, K., Cowan, P., d'Apice, A., Dwyer, K., Rosenberg, R., et al. (2011). Impact of CD39 and purinergic signalling on the growth and metastasis of colorectal cancer. Purinergic Signal. *7*, 231–241.

Larrick, J.W., Alfenito, M.R., Scott, J.K., Parren, P.W., Burton, D.R., Bradbury, A.R., Lemere, C.A., Messer, A., Huston, J.S., Carter, P.J., et al. (2016). Antibody Engineering & Therapeutics 2016: The Antibody Society's annual meeting, December 11-15, 2016, San Diego, CA. MAbs *8*, 1425–1434.

Lartigue, A., Gruez, A., Briand, L., Pernollet, J.C., Spinelli, S., Tegoni, M., and Cambillau, C. (2003). Optimization of crystals from nanodrops: crystallization and preliminary crystallographic study of a pheromone-binding protein from the honeybee Apis mellifera L. Acta. Crystallogr. D. Biol. Crystallogr. *59*, 919–921.

Ludtke, S.J., Baldwin, P.R., and Chiu, W. (1999). EMAN: semiautomated software for high-resolution single-particle reconstructions. J. Struct. Biol. *128*, 82–97.

Michaud, M., Martins, I., Sukkurwala, A.Q., Adjemian, S., Ma, Y., Pellegatti, P., Shen, S., Kepp, O., Scoazec, M., Mignot, G., et al. (2011). Autophagy-dependent anticancer immune responses induced by chemotherapeutic agents in mice. Science *334*, 1573–1577.

Nikolova, M., Carriere, M., Jenabian, M.A., Limou, S., Younas, M., Kök, A., Huë, S., Seddiki, N., Hulin, A., Delaneau, O., et al. (2011). CD39/adenosine pathway is involved in AIDS progression. PLoS Pathog. *7*, e1002110.

Okazaki, T., Chikuma, S., Iwai, Y., Fagarasan, S., and Honjo, T. (2013). A rheostat for immune responses: the unique properties of PD-1 and their advantages for clinical application. Nat. Immunol. *14*, 1212–1218.

Overman, M.J., LoRusso, P., Strickler, J.H., Patel, S.P., Clarke, S.J., Noonan, A.M., Prasanna, T., Amin, M.A., Nemunaitis, J.J., Desai, J., et al. (2018). Safety, efficacy and pharmacodynamics (PD) of MEDI9447 (oleclumab) alone or in combination with durvalumab in advanced colorectal cancer (CRC) or pancreatic cancer (panc). Journal of Clinical Oncology *36*, 4123.

Palucka, A.K., and Coussens, L.M. (2016). The Basis of Oncoimmunology. Cell *164*, 1233–1247.

Sharma, P., and Allison, J.P. (2015a). The future of immune checkpoint therapy. Science *348*, 56–61.

Sharma, P., and Allison, J.P. (2015b). Immune checkpoint targeting in cancer therapy: toward combination strategies with curative potential. Cell *161*, 205–214.

Sharma, P., Hu-Lieskovan, S., Wargo, J.A., and Ribas, A. (2017). Primary, Adaptive, and Acquired Resistance to Cancer Immunotherapy. Cell *168*, 707–723.

Silva-Vilches, C., Ring, S., and Mahnke, K. (2018). ATP and Its Metabolite Adenosine as Regulators of Dendritic Cell Activity. Front. Immunol. *9*, 2581.

Simoni, Y., Becht, E., Fehlings, M., Loh, C.Y., Koo, S.L., Teng, K.W.W., Yeong, J.P.S., Nahar, R., Zhang, T., Kared, H., et al. (2018). Bystander $CD8^+$ T cells are abundant and phenotypically distinct in human tumour infiltrates. Nature *557*, 575–579.

Siu, L.L., Burris, H., Le, D.T., Hollebecque, A., Steeghs, N., Delord, J.-P., Hilton, J., Barnhart, B., Sega, E., Sanghavi, K., et al. (2018). Abstract CT180: Preliminary phase 1 profile of BMS-986179, an anti-CD73 antibody, in combination with nivolumab in patients with advanced solid tumors. Cancer Res. *78*, CT180.

Stagg, J., Divisekera, U., Duret, H., Sparwasser, T., Teng, M.W., Darcy, P.K., and Smyth, M.J. (2011). CD73-deficient mice have increased antitumor immunity and are resistant to experimental metastasis. Cancer Res. *71*, 2892–2900.

Stagg, J., Beavis, P.A., Divisekera, U., Liu, M.C., Möller, A., Darcy, P.K., and Smyth, M.J. (2012). CD73-deficient mice are resistant to carcinogenesis. Cancer Res. *72*, 2190–2196.

Sun, X., Wu, Y., Gao, W., Enjyoji, K., Csizmadia, E., Müller, C.E., Murakami, T., and Robson, S.C. (2010). CD39/ENTPD1 expression by CD4+Foxp3+ regulatory T cells promotes hepatic metastatic tumor growth in mice. Gastroenterology *139*, 1030–1040.

Sun, X., Han, L., Seth, P., Bian, S., Li, L., Csizmadia, E., Junger, W.G., Schmelzle, M., Usheva, A., Tapper, E.B., et al. (2013). Disordered purinergic signaling and abnormal cellular metabolism are associated with development of liver cancer in Cd39/ENTPD1 null mice. Hepatology *57*, 205–216.

Vagin, A., and Teplyakov, A. (2010). Molecular replacement with MOLREP. Acta Crystallogr. D Biol. Crystallogr. *66*, 22–25.

Waickman, A.T., Alme, A., Senaldi, L., Zarek, P.E., Horton, M., and Powell, J.D. (2012). Enhancement of tumor immunotherapy by deletion of the A2A adenosine receptor. Cancer Immunol. Immunother. *61*, 917–926.

White, N., and Burnstock, G. (2006). P2 receptors and cancer. Trends Pharmacol. Sci. *27*, 211–217.

Winn, M.D., Ballard, C.C., Cowtan, K.D., Dodson, E.J., Emsley, P., Evans, P.R., Keegan, R.M., Krissinel, E.B., Leslie, A.G., McCoy, A., et al. (2011). Overview of the CCP4 suite and current developments. Acta Crystallogr. D Biol. Crystallogr. *67*, 235–242.

Young, A., Ngiow, S.F., Barkauskas, D.S., Sult, E., Hay, C., Blake, S.J., Huang, Q., Liu, J., Takeda, K., Teng, M.W.L., et al. (2016). Co-inhibition of CD73 and A2AR Adenosine Signaling Improves Anti-tumor Immune Responses. Cancer Cell *30*, 391–403.

STAR★METHODS

KEY RESOURCES TABLE

REAGENT or RESOURCE	SOURCE	IDENTIFIER
Antibodies		
IPH5201 (humanized anti-human CD39 antibody, human IgG1 backbone, Fc silent)	Innate Pharma	Patent#WO 2018/167267 Al
moIPH5201 (murinized anti-human CD39 antibody, mouse IgG1 backbone, Fc silent)	Innate Pharma	Patent#WO 2018/167267 Al
BY40 (humanized anti-CD39 antibody, human IgG1 backbone, Fc silent)	Innate Pharma	Patent#WO2009/095478 A1
IPH5301 (humanized anti-CD73 antibody, human IgG1 backbone, Fc silent)	Innate Pharma	Patent#WO2016/055609 A1
MEDI9447 (human anti-CD73 antibody, human IgG1, Fc silent)	Innate Pharma	Patent#WO2016/075099 A1
CD73.4 (human anti-CD73 antibody, human IgG1-IgG2 chimera, Fc silent)	Innate Pharma	Patent#WO2016/081748 A3
Human IgG1 control Ab (Fc silent)	Innate Pharma	N/A
Mouse IgG1 Control Ab (Fc silent)	Innate Pharma	N/A
Anti-human CD83-PE	Beckman Coulter	Cat#IM2218U
Anti-human HLA-DR-BV510	BioLegend	Cat#307646; RRID:AB_2561948
Anti-human CD3-BUV737	BD Biosciences	Cat#564307; RRID:AB_2744390
Anti-human CD8-BV786	BD Biosciences	Cat#563823; RRID:AB_2687487
Anti-human CD45-BV711	BioLegend	Cat#304050; RRID:AB_2563466
Anti-human CD4-Alexa700	BD Biosciences	Cat#557922; RRID:AB_396943
Anti-human PD-1-APC-Cy7	BioLegend	Cat#329922; RRID:AB_10933429
Anti-human CD39-APC	BioLegend	Cat#328210; RRID:AB_1953234
Mouse Fc block	BD Biosciences	Cat#553142; RRID:AB_394657
Anti-mouse CD3-BV711	BD Biosciences	Cat#563123; RRID:AB_2687954
Anti-mouse CD11b-V500	BD Biosciences	Cat#562127; RRID:AB_10893815
Anti-mouse CD45-BV605	BD Biosciences	Cat#563053; RRID:AB_2737976
Anti-mouse Ly6C-BV421	BD Biosciences	Cat#562727; RRID:AB_2737748
Anti-mouse NKp46-AF647 (clone 29A1.4)	Innate Pharma	N/A
Anti-mouse CD4-BUV737	BD Biosciences	Cat#564933; RRID:AB_2732918
Anti-mouse CD25-PE-Cy7	BD Biosciences	Cat#552880; RRID:AB_394509
Anti-mouse CD19-FITC	BD Biosciences	Cat#553785; RRID:AB_395049
Aqua Live Dead	ThermoFisher Scientific	Cat#L34966
Anti-human IgG Fc fragment-HRP	Bethyl	Cat#A80-248P; RRID:AB_10630712
Anti-mouse IgG Fc fragment-HRP	Bethyl	Cat#A90-239P; RRID:AB_10630447
Mouse anti-human CD45-APC-Cy7 (clone 2D1)	BD Biosciences	Cat#557833; RRID:AB_396891
Mouse anti-human CD3-PerCP (clone SK7)	BD Biosciences	Cat#345766; RRID:AB_2783791
Mouse anti-human CD4-BV650 (clone SK3)	BD Biosciences	Cat#563875; RRID:AB_2744425
Mouse anti-human CD8-BV605 (clone SK1)	BD Biosciences	Cat#564115; RRID:AB_2744466
Mouse anti-human CD25-AF700 (clone M-A251)	BD Biosciences	Cat#561398; RRID:AB_10643605
Mouse anti-human CD73-BV421 (clone AD2)	BD Biosciences	Cat#562430; RRID:AB_11153119
Mouse anti-human CD39-PE (clone TU66)	BD Biosciences	Cat#555464; RRID:AB_395856
Mouse anti-human CD279/PD-1-AF647 (clone EH12.1)	BD Biosciences	Cat#560838; RRID:AB_2033988
Mouse anti-human CD366/Tim3-PE-Cy7 (clone F38-2E2)	eBioscience	Cat#25-3109-42; RRID:AB_2573438
Rat anti-human FoxP3-AF488 (clone PCH101)	eBioscience	Cat#53-4776-42; RRID:AB_11043133
Rat anti-mouse CD19-AF700 (clone 1D3)	BD Biosciences	Cat#557958; RRID:AB_396958

(*Continued on next page*)

Continued

REAGENT or RESOURCE	SOURCE	IDENTIFIER
Rat anti-mouse CD25-PE-Cy5 (clone PC61)	BioLegend	Cat#102010; RRID:AB_312859
Hamster anti-mouse CD3e-PE-Cy5 (clone 145-2C11)	BD Biosciences	Cat#553065; RRID:AB_394598
Rat anti-mouse CD39-PE-Cy7 (clone 24DMS1)	eBioscience	Cat#25-0391-82; RRID:AB_1210766
Rat anti-mouse CD4-BV605 (clone RM4-5)	BD Biosciences	Cat#563151; RRID:AB_2687549
Rat anti-mouse CD45-BV650 (clone 30-F11)	BD Biosciences	Cat#563410; RRID:AB_2738189
Rat anti-mouse CD8a-AF700 (clone 53-6.7)	eBioscience	Cat#56-0081-82; RRID:AB_494005
Rat anti-mouse CD11b-APC (clone M1/70)	BD Biosciences	Cat#553312; RRID:AB_398535
Anti-mouse CD11c-PE-Vio770 (clone N418)	Miltenyi Biotec	Cat#130-107-139; RRID:AB_2660160
Rat anti-mouse CD73-BV605 (clone TY/11.8)	BioLegend	Cat#127215; RRID:AB_2561528
Rat anti-mouse F4/80-APC-eFluor780 (clone BM8)	eBioscience	Cat#47-4801-82; RRID:AB_2735036
Rat anti-mouse FoxP3-APC (clone FJK-16S)	eBioscience	Cat#17-5773-82; RRID:AB_469457
Rat anti-mouse Gr1-AF700 (clone RB6-8C5)	BD Biosciences	Cat#557979; RRID:AB_396971
Rat anti-mouse IFN gamma-BV421 (clone XMG1.2)	Biolegend	Cat#505829; RRID:AB_10897937
Rat anti-mouse IL2-APC-Cy7 (clone JES6-5H4)	BD Biosciences	Cat#560547; RRID:AB_1727544
Anti-mouse MHCII-VioBlue (clone M5/114.15.2)	Miltenyi Biotec	Cat#130-102-145; RRID:AB_2660060
Rat anti-mouse NKP46-V450 (clone 29A1.4)	BD Biosciences	Cat#560763; RRID:AB_1727469
Hamster anti-mouse PD1-FITC (clone J43)	eBioscience	Cat#11-9985-85; RRID:AB_465473
Hamster anti-mouse TCR gd-BV605 (clone GL3)	Biolegend	Cat#118129; RRID:AB_2563356
Rat anti-mouse Tim3-PE (clone RMT3-23)	eBioscience	Cat#12-5870-83; RRID:AB_465975
Human Fc block	BD Biosciences	Cat#5642219; RRID:AB_2728082
Mouse anti-human CD3-Purified (clone UCHT1)	BD Biosciences	Cat#555329; RRID:AB_395736
Mouse anti-human CD28-Purified (clone CD28.2)	BD Biosciences	Cat#555725; RRID:AB_396068
Hamster anti-mouse CD3-Purified (clone 145.2C11)	BD Biosciences	Cat#550275; RRID:AB_393572
Hamster anti-mouse CD28-Purified (clone CD28.2)	BD Biosciences	Cat#553294; RRID:AB_394763
Mouse anti-human CD39-Purified, IHC/IF (clone 22A9)	Abcam	Cat#ab108248; RRID:AB_10890104
Rabbit anti-human PD-1-Purified, IHC (clone EP239)	BioSB	Cat#BSB 3153
Rabbit anti-human PD-1-Purified, IHC (clone MRQ22)	Abcam	Cat#ab137132
Rat Anti-mouse PD-1 (clone RMP1-14), *in vivo* use	BioXcell	Cat#BE0146; RRID:AB_10949053
Rat IgG2a (clone RMP1-14), *in vivo* use	BioXcell	Cat#BE0089; RRID:AB_1107769
Syrian hamster anti-mouse CTLA-4 (clone 9H10), *in vivo* use	BioXcell	Cat#BP0131; RRID:AB_10950184
Polyclonal Syrian hamster IgG, *in vivo use*	BioXcell	Cat#BP0087; RRID:AB_1107782
Rat anti-mouse CD8 (clone 2.43), *in vivo* use	BioXcell	Cat#BP0061; RRID:AB_1125541
Rat IgG2b (clone LTF-2), *in vivo* use	BioXcell	Cat#BP0090; RRID:AB_1107780
Rat anti-mouse CD4 (clone GK1.5), *in vivo* use	BioXcell	Cat#BP0003; RRID:AB_1107636
Mouse anti-mouse NK1.1 (clone PK136), *in vivo* use	BioXcell	Cat#BP0036; RRID:AB_1107737
Mouse IgG2a (clone C1.18.4), *in vivo* use	BioXcell	Cat#BP0085; RRID:AB_1107771
Donkey anti-mouse IgG (H+L)-AF647	ThermoFisher Scientific	Cat#A31-571; RRID:AB_162542
Donkey anti-rabbit IgG (H+L)-AF488	ThermoFisher Scientific	Cat#A21-206; RRID:AB_2535792
Biological Samples		
Melanoma, ovary and sarcoma human biopsies	Centre Hospitalier Régional Universitaire de Montpellier/ Institut regional du cancer de Montpellier	N/A
Fresh biopsies and matched blood from melanoma patients	Centre Hospitalier Régional Universitaire de Montpellier/ Institut regional du cancer de Montpellier	N/A

(*Continued on next page*)

Continued

REAGENT or RESOURCE	SOURCE	IDENTIFIER
Melanoma FFPE	Centre Hospitalier Regional Universitaire de Montpellier / Institut regional du cancer de Montpellier	BIOBANK BB-033-00031
Human whole blood or buffy coats	French Blood Agency, Marseille	Cat#B3111
Frozen PBMC from Breast cancer patients	Center for cancer research, Marseille	N/A
Fresh Biopsies and matched blood from SCCHN patients	Institut Curie (Paris, France)	N/A
Chemicals, Peptides, and Recombinant Proteins		
Recombinant human CD39 (ENTPD1)	Innate Pharma	UniProt accession#P49961
Adenosine 5′-triphosphate disodium salt hydrate	Sigma-Aldrich	Cat#A26209; CAS#34369-07-8
Adenosine 5′-monophosphate monohydrate	Sigma-Aldrich	Cat#A2252; CAS#18422-05-4
Recombinant human GM-CSF, premium grade	Miltenyi Biotec	Cat#130-093-867
Recombinant human IL-4, premium grade	Miltenyi Biotec	Cat#130-093-920
LPS (ultrapure from *E. Coli* K12 strain)	InvivoGen	Cat#tlrl-peklps; EC#1272/2008
Oxaliplatin	Fresenius kabi	CAS#61825-94-3
Recombinant human CD39 (ENTPD1)	Bio-Techne	Cat#4397-EN
Recombinant human CD39L1 (ENTPD2)	Bio-Techne	Cat#6087-EN
Recombinant human CD39L2 (ENTPD6)	Bio-Techne	Cat#4399-EN
Recombinant human CD39L3 (ENTPD3)	Bio-Techne	Cat#4400-EN
Recombinant human CD39L4 (ENTPD5)	Bio-Techne	Cat#5297-EN
Protein-A	GE Healthcare	Cat#17-0872-50
CM5 sensor chip	GE Healthcare	Cat#BR-1005-30
Amine coupling kit (EDC/NHS)	GE Healthcare	Cat#BR-1000-50
ARL67156 trisodium salt (CD39 inhibitor)	Trocis	Cat#1283; CAS#1021868-83-6
Collagenase IV	Sigma-Aldrich	Cat#C5138
DNase I	Sigma-Aldrich	Cat#11284932001
PMA	Sigma-Aldrich	Cat#P1585; CAS#16561-29-8
Ionomycin calcium salt	Sigma-Aldrich	Cat#I3909; EC#1907/2006
PNGase F *Elizabethkingia meningoseptica*	Sigma-Aldrich	Cat#F8435; CAS#83534-39-8
Succinic acid	Sigma-Aldrich	Cat#S3674; CAS#110-15-6
Poluethylene glycol 3350	Sigma-Aldrich	Cat#1546547; CAS#25322-68-3
Uranyl formate	Polysciences	Cat#24762; CAS#16984-59-1
Critical Commercial Assays		
Mouse Foxp3 Buffer Set	BD Biosciences	Cat#560409
Kit Envision Flex	Agilent	Cat#K8000
AEC substrate solution	Zytomed systems	Cat#ZUC042; EC#205-057-7
Mounting Solution Mowiol® 4-88	Sigma-Aldrich	Cat#81381
Protein Block	Agilent	Cat#X0909
CellTiter Glo luminescent assay	Promega	Cat#G7573
AMP Glo luminescent assay	Promega	Cat#V5011
CD14 microbeads, human	Miltenyi Biotec	Cat#130-050-201
CD4+ T cell isolation kit, human	Miltenyi Biotec	Cat#130-096-533
Dynabeads CD3/CD28 T cell expander	ThermoFisher Scientific	Cat#11131D
CellTrace Violet cell proliferation kit	ThermoFisher Scientific	Cat#C34557
Human IL-1β ELISA	BioLegend	Cat#437004
Deposited Data		
Structure of human CD73 in complex with IPH5301 Ab	This paper	PDB: 6HXW

(*Continued on next page*)

Continued

REAGENT or RESOURCE	SOURCE	IDENTIFIER
Experimental Models: Cell Lines		
Mouse B16F10	ATCC	Cat#CRL-6475; RRID:CVCL_0159
Mouse MCA205	Courtesy from Dr Kroemer (Centre de Recherche des Cordeliers, Paris, France.)	http://www.kroemerlab.com/
Mouse MC38	Courtesy from Dr Cavaillès (Institut de recherche en cancérologie de Montpellier, France.)	https://ircm.fr/index.php?pagendx=40
Human WIL2-NS	ECACC	Cat#90112121; RRID:CVCL_2761
Human Mino	DSMZ	Cat#ACC-687; RRID:CVCL_1872
Human A375	ATCC	Cat# CRL-1619, RRID:CVCL_0132
Human MDA-MB-231	ATCC	Cat# HTB-26; RRID:CVCL_0062
Experimental Models: Organisms/Strains		
Mouse C57BL/6N wild type	Charles River/Envigo	N/A
Mouse C57BL/6N CD39KO	Innate Pharma	N/A
Human CD39 KI mice (B6-Entpd1tm1Ciphe)	Innate Pharma	N/A
Software and Algorithms		
Prism V7	GraphPad	https://www.graphpad.com/
FlowJo 10	Tristar	https://www.flowjo.com/
4000 Series Explorer software	Applied Biosystems	N/A
Biacore T200 Sotfware V3	GE Healthcare	N/A
XDS	Kabsch, 2010	N/A
SCALA	Evans, 2006	N/A
CCP4	Winn et al., 2011	N/A
MolREP	Vagin and Teplyakov, 2010	N/A
AutoBuster	Blanc et al., 2004	N/A
COOT	Emsley and Cowtan 2004	N/A
Eman2	Ludtke et al., 1999	N/A
Molprobity	Chen et al., 2010	N/A
Other		
GentleMACS dissociator	Miltenyi Biotec	Cat#130-093-235
BD Fortessa cell analyzer	Beckton Dickinson	N/A
CytoFlex cell analyzer	Beckman Coulter	N/A
4800 Plus MALDI-TOF/TOF Proteomics Analyzer	ABSciex	N/A
Autostainer Link 48	Dako	N/A
Axio Imager M2	Zeiss	N/A
Biacore T200	GE Healthcare	N/A
Enspire multimode plate reader	Perkin Elmer	N/A
His Trap Excel	Sigma-Aldrich	Cat#GE17-3712-06
Hiload superdex 200pg 16/600	Sigma-Aldrich	Cat#GE28-9893-35
Superose6 10/300GL Increase	Sigma-Aldrich	Cat#GE29-0915-96
Mono S 4.6/100PE	Sigma-Aldrich	Cat#GE17-5180-01
Grid Formvar/carbon on 300mesh copper	Agar scientific	Cat#AGS162

CONTACT FOR REAGENT AND RESOURCE SHARING

Further information and requests for reagents may be directed to and will be fulfilled by the Lead Contact, Eric Vivier (vivier@ciml.univ-mrs.fr).

EXPERIMENTAL MODEL AND SUBJECT DETAILS

Human Subjects

Fresh biopsies and matched blood from melanoma patients were obtained at the time of surgical resection under Centre Hospitalier Régional Universitaire de Montpellier approved protocol and written informed consent from each patient. Patients' characteristics are summarized in Tables S1 and S3.

Peripheral blood and tumor tissues from SCCHN patients were obtained at the time of surgical resection under Institut Curie approved protocol and written informed consent from each patient. Patients' characteristics are summarized in Table S2.

Fresh ovary cancer and sarcoma specimens were provided by the Institut Régional du Cancer de Montpellier (BioBank #BB-033-0059) under an approved protocol and written informed consent from each patient. Patients' characteristics are summarized in Table S3.

Frozen PBMC from breast cancer patients were obtained under Institut Paoli Calmette approved protocol and written informed consent from each patient. Patients' characteristics are summarized in Table S5.

Peripheral blood samples from healthy donors were obtained from Etablissement Francais du Sang (EFS, Marseille) under a written consent obtained from each volunteer.

Formalin-fixed paraffin-embedded tissue sections from melanoma patients were provided by Prof. Sylvain Lehmann, the director of the BB-033-00031 Biobank at the Centre Hospitalier Régional Universitaire de Montpellier.

Mice

CD39-deficient mice (C57BL/6N), generated by OREGA Biotech, were bred and kept under specific and opportunistic pathogen-free conditions at the Charles River animal facility. C57BL/6N mice were purchased from Envigo or Charles River. For experiments, mice were kept in specific pathogen-free conditions in the animal facilities of the Institut de Recherche sur le Cancer de Montpellier. All procedures for animal handling and experiments were approved by the ethics committee of the local animal facility ("ComEth") and the institutional review board, under the authority of the regional ethics committee for animal experimentation.

Human CD39 KI mice (B6-Entpd1tm1Ciphe) were generated at UMS-CIPHE (Marseille, France) with the following strategy: briefly, the human cDNA sequence coded by exons 2-10 were placed with the 2nd exon of the mouse CD39 gene. Chimeric germline transmitting HE mice were crossed to generate HO human CD39ki mice, and further backcrossed under 6 generations with C57BL/6N mice. Human CD39 ki mice were further bred at the CIPHE animal facility (Marseille) under specific pathogen free conditions. For tumor experiments, female mice were used at 6 to 12 weeks of age, kept under specific and opportunistic pathogen free conditions at Innate Pharma animal facility (Marseille). All animal experiments were performed in accordance with the rules of the Innate Pharma ethics and animal welfare committees.

Cell lines

B16F10 and MCA205 cells were maintained in complete DMEM (GE Healthcare Life Sciences) supplemented with 10% fetal calf serum (FCS), and 2 mg/ml gentamycin (Life Technologies). MC38 cells were grown in complete RPMI 1640 medium supplemented with 10% FCS, 16 mM HEPES (Life Technologies) and 2 mg/ml gentamycin. WIL2-NS and Mino cell lines were maintained in RPMI 1640 medium supplemented with 10% FCS, 1% GlutaMAX and 1% Sodium Pyruvate (all from Life Technologies). A375 and MDA-MB-231 were grown in DMEM medium supplemented with 10% FCS, 1% L-Glutamine 200 mM and 1% Sodium Pyruvate (all from Life Technologies). All cell lines were cultured at 37°C under an atmosphere containing 5% CO_2. All cell lines were tested regularly for mycoplasma contamination, and the murine cell lines used for tumor grafts were also regularly tested for rodent pathogens.

METHOD DETAILS

Antibody cloning, chimerization and purification

The cloning vector used in this study is the Selexis mammalian expression vector plasmid. mRNA of IPH5201 and IPH5301 hybridomas were purified and cDNA were generated to perform PCR with pools of primers allowing the amplification of VH and VL sequences of mouse variable domains. The VH purified PCR products were then cloned into the SLX HUB3 vector. This vector contains a human IgG1 sequence harboring 5 mutations that abrogate FcR binding (L234A/L235E/G237A/A330S/ P331S). The VL purified PCR products were cloned into the SLX HuCk vector. PCR were performed on the bacterial colonies obtained after the In-Fusion ligations and the selected positive clones were prepared as miniprep and sequenced. VH and VL plasmids were transfected in CHO cell line according the standard nucleofection protocol (Amaxa, 4D-Nucleofector). After 7 days of culture, supernatants were harvested and the antibodies purified onto protein-A Sepharose beads.

The VH and VL chains of the isotype control antibody were selected from an antibody that binds a toxin produced by a Mexican Scorpio. MEDI9447 (MedImmune) and CD73.4 (Brystol Meyer Squibb) mAbs were cloned using the VH and VL chain sequences published in #WO 2016/075099 Al and #WO 2016/081748 A3 application patents, respectively. All VH and VL sequences were chemically synthesized. The control Ab was cloned into the SLX HUB3 (VH) and SLX HuCk (VL) vectors. MEDI9447 was cloned into the SLX

HUB3 (VH) and SLX HuCl (VL) vectors. CD73.4 was cloned into SLX HUG2G1 (VH) and SLX HuCk (VL) vectors. The HUG2G1 vector contains a human IgG1 sequence harboring 2 mutations that abrogates FcR binding (A330S/ P331S) and the CH1 + Hinge region of an IgG2 that contains a mutation in position 219 (C219S).

Flow cytometry

For immunophenotyping, cells were incubated with either mouse or human blocking buffer (Miltenyi Biotec) for 20 min at 4°C in FACs buffer, pelleted and resuspended in appropriate antibody cocktail for 1 h at 4°C. Cells were then fixed and permeabilized with the corresponding buffer and stained for intracellular protein detection for 1 h for human cells or overnight for mouse cells, at 4°C in the dark. Cells were finally fixed with 1% PFA in PBS and stored until acquisition with a Fortessa or Cytoflex flow cytometer. Data were analyzed with Flowjo 10 software.

To assess Ab-mediated CD39 or CD73 down-modulation, 10^5 WIL2-NS, A375 and MDA-MB-231 cell lines were distributed into round-bottom 96W-microplates in presence of 10 μg/ml anti-CD39 (WIL2-NS) or anti-CD73 (A375, MDA-MB-231) Abs. Cells were incubated for a time-course at 4°C and 37°C and at the different time-points, cells were recovered, washed twice in staining buffer and incubated for 30 additional minutes with a fixed dose of the same Ab used for the time-course. Bound Abs were revealed with a PE or APC-conjugated goat anti-human IgG Fc secondary Abs for 20 min at 4°C. Cells were then analyzed on a Fortessa flow cytometer. The relative expression of CD39 and CD73 was determined using the first-time point as reference and plotted versus time on graphs using GraphPad Prism program.

Murine tumor models and treatments

$5x10^4$ B16F10 or $5x10^5$ MC38 or 10^6 MCA205 cells resuspended in 100 μl of PBS were injected subcutaneously (s.c.) into 9- to 12-week-old WT or CD39-deficient female mice. Tumor growth was monitored three times per week with a caliper and mice were killed when the tumor reached a volume of 1500 mm^3. Tumor volume was calculated with the following formula: length x width x width/2. For assessment of the therapeutic effect of oxaliplatin, MCA205-grafted mice received a single intraperitoneal (i.p.) injection of oxaliplatin, at a dose of 10 mg/kg, on day 5. For assessment of the therapeutic effect of anti-PD-1 mAb, B16F10-grafted mice received six injections of anti-PD-1 antibody (i.p. injection, 200 μg/mouse) or control rIgG2A antibody (i.p. injection, 200 μg/mouse), on days 6, 9, 13, 16, 20 and 23. For assessment of the therapeutic effect of anti-CTLA-4 mAb, B16F10-grafted mice received eight injections of anti- CTLA-4 antibody (i.p. injection, 200 μg/mouse) or control antibody (i.p. injection, 200 μg/mouse), on days 5, 8, 12, 16, 19, 23, 26 and 30. We evaluated the effect of anti-PD-1 therapy in MCA205-grafted mice, by administering eight injections of anti-PD-1 antibody or control rIgG2A antibody on days 6, 9, 13, 16, 20, 23, 27 and 30. CD8 T cells were depleted by an injection of anti-CD8 antibody (i.p. injections, 200 μg/mouse), and then further injections twice weekly, and the results were compared with those of mice receiving control rIgG2b antibody (i.p. injections, 200 μg/mouse, BioXCell, BP0090) according to the same schedule. CD4 T cells were depleted by the injection of anti-CD4 mAb (i.p. injections, 200 μg/mouse, BioXCell, BP0003) on day 4 and then once weekly, and comparisons were made with control mIgG2a antibody (i.p. injections, 200 μg/mouse, BioXCell, BP0085). NK cells were deleted by the injection of anti-NK antibodies (i.p. injections, 200 μg/mouse, BioXCell, BP0036) on day 4 and then twice weekly, with comparison against control mIgG2a antibody (i.p. injections, 200 μg/mouse, BioXCell, BP0085). CD8, CD4 and NK cell depletions were checked by FACS analysis at the time of death of the mouse.

Human CD39 KI mice were treated with IPH5201 and control Ab (i.v. injections; 400 μg/mouse) or left untreated. 20 hours post-injection, spleens were collected and splenocytes were isolated by mechanical dissociation. Spleen cells or the dissociation supernatant were incubated with 20 μM ATP for 2 hours (cells) or 30 min (supernatant) at 37°C. 50 μl of supernatant of both conditions were transferred in white well plates for the quantification of residual ATP using Cell Titer Glo assay. WT and mouse CD39 KO mice were used as control. ATP in absence or presence of cells or supernatants were plotted on graphs using GraphPad Prism software.

In order to assess anti-tumor effect of IPH5201 and oxaliplatin *in vivo*, human CD39 KI mice were i.p. grafted with $1x10^6$ MCA205 cells in PBS (100 μl/mouse). Then, the mice received 8 i.v. injections of IPH5201 or control Ab (400 μg/mouse for the 1st injection, 200 μg/mouse all others; day 4, 7, 11, 14, 19, 22, 26, 29) and 2 i.p. injections of Oxaliplatin (10 mg/kg; day 5 and 12 or 14). Tumor growth was monitored three times a week and mice were euthanized when the tumor reached a volume of 2000 mm^3 or in case of tumor necrosis. Tumor volume was calculated as previously mentioned. Tumor volume or percent of survival versus time were plotted on graphs using GraphPad Prism software.

AMP determination by MALDI-TOF spectrometry

Cells were washed in cold PBS and resuspended in PBS supplemented with 50 μM ATP in the presence or absence of CD39 inhibitors (ARL67156 100 μM, CD39 antibodies or isotype controls at 15 μg/ml) for 30 minutes at 4°C. After centrifugation, the AMP levels in the supernatant were determined by mass spectrometry. Briefly, an internal standard working solution was prepared by directly mixing GMP (m/z = 364.06) with matrix solution (5 mg/ml cyano-4-hydroxycinnamic solved in 70% acetonitrile/0.1% TFA). Equal volumes of analyte and internal standard solutions were mixed and two microliters of the mixture was spotted in triplicate onto the MALDI-TOF target plate. For each spot, a 4800 Plus MALDI-TOF/TOF Proteomics Analyzer was used to acquire 40 mass spectra automatically (50 shots/spectrum) in positive reflector ion mode in the m/z 250-370 range. For quantitative measurements, the laser power was adjusted automatically to prevent signal saturation. Only spectra for which the maximum peak height was within a specific interval were retained. The spectra were averaged and the analyte/internal standard peak area ratios were calculated as response

factors, by averaging four measurements. A calibration curve obtained with pure AMP (10-50 μM) was used to calculate the concentration in each sample. Results are expressed as the fold-increase in AMP levels relative to ATP alone or as percentage inhibition of AMP generation relative to isotype control conditions.

Isolation of immune cells

Spleens and tumors were recovered in ice-cold PBS supplemented with 0.5% BSA and 2 mM EDTA (dissociation buffer) and were mechanically dissociated. For spleens, red blood cells were eliminated by adding 2 mL ACK lysing buffer. White blood cells were recovered by centrifugation, washed with PBS and resuspended in RPMI 1640 plus 10% FCS for functional assays or in flow cytometry buffer (2% FCS, 0.5 M EDTA, 0.02% NaN3 in PBS) for staining and flow cytometry analysis. Human tissues, MCA205 and MC38 tumors were minced to generate 2 μm^3 fragments, which were treated with collagenase IVs (200 μg/ml for mouse tissues, 1 mg/ml for human tissues) and DNase (50 U/ml) in Hank's balanced salt solution for 1 hour at 37°C in C Tubes (Miltenyi Biotec). Mechanical dissociation was performed simultaneously, with a gentleMACS dissociator, according to the appropriate preprogrammed protocol provided by the manufacturer. After dissociation, the tumor cells were passed through filters with 70 μm and 40 μm pores (Falcon; Cell Strainerr) and centrifuged. Pellets were resuspended in RPMI 1640 plus 10% FCS for functional assays or in flow cytometry buffer for staining and flow cytometry.

Blockade of membrane-associated CD39 or CD73 activity

WIL2-NS and Mino cell lines were plated in TBS in presence of a dose range of anti-CD39 Abs for a 1 hour incubation period at 37°C. 20 μM ATP were added to the cells for 1-additional hour at 37°C. Supernatants were transferred into 96W white microplates (Greiner Bio One) and CellTiter Glo™ was added to the plates. Emitted light was measured on an Enspire plate reader.

A375 and MDA-MB-231 cell lines were plated in TBS in presence of a dose range of anti-CD73 Abs for a 1 hour incubation period at 4°C. 12.5 μM AMP were added to the cells for 1-additional hour at 4°C. Supernatants were transferred into 96W white microplates and residual AMP was quantified using the AMP Glo™ assay. Emitted light was measured on an Enspire plate reader. Residual ATP or AMP versus Ab concentration were plotted on graphs and EC_{50} were calculated using GraphPad Prism software.

The percentage of enzymatic activity inhibition was calculated as described below:

$$\frac{(Cells + AT(M)P + Ab) - (Cells + AT(M)P)}{(AT(M)P) - (Cells + AT(M)P)} \times 100$$

Blockade of soluble CD39 or CD73 activity

WIL2-NS and Mino cell lines (10^6 cells/ml) were cultured for 24 h at 37°C then cell supernatants (SN) were carefully picked-up, centrifuged at 140 g for 10 min at RT, transferred into new tubes and centrifuged at 368 g for 10 min at RT. SN were distributed in 96-well flat-bottom plates in presence of anti-CD39 Ab dose-ranges and incubated for 1 hour at 37°C. 20 μM ATP were added and plates were incubated 2h at 37°C. The reactional medium was transferred into Microclear-96 plates and residual ATP was quantified using the CellTiter Glo™ assay. A375 and MDA-MB-231 cell lines ($1.2x10^6$ and $2.4x10^6$ cell/cm^2, respectively) were cultured for 36 h at 37°C then cell supernatants (SN) were carefully picked-up, centrifuged twice at 3000 g for 5 min at RT. SN were distributed in 96-well flat-bottom plates in presence of anti-CD73 Ab dose-ranges and incubated for 1 hour at 37°C. 200 μM AMP were added and plates were incubated 2 h at 37°C. The reactional medium was transferred into Microclear-96 plates and residual AMP was quantified using the AMP Glo™ assay. In both assays, luminescence was quantified on an Enspire plate reader. Residual ATP/AMP versus Ab concentration was plotted on graphs using GraphPad Prism software. The percentage of enzymatic activity inhibition was calculated as previously described by replacing cells by SN in the formula.

In vitro enzymatic assay on recombinant soluble CD39

50 to 800 ng/ml of recombinant human CD39 were incubated in white 96W flat-bottom microplates in the presence of a dose range of anti-CD39 or isotype control Abs or ARL67156 chemical inhibitor. Plates were incubated for 1h at 37°C. Depending on the experiment, 12.5 μM or 20 μM ATP were added to each well and plates were incubated at 37°C for 30 supplemental minutes. Luciferase/luciferin-containing CellTiter Glo was added into wells, plates were incubated for 5 minutes at RT in the dark and emitted light was measured using an Enspire plate reader. Luminescence units versus anti-CD39 Ab concentration was plotted in graphs using GraphPad Prism software.

T cell proliferation assay

Peripheral blood from healthy donors was obtained from the EFS and mononuclear cells were isolated on a Ficoll gradient. Lymphocytes were further enriched on a 52% Percoll gradient (cell pellets) and stained with a 2 μM CellTrace Violet (Thermofisher, #C34557). $5x10^4$ to $1x10^5$ of stained cells were distributed in 96w round-bottom plates, incubated for 1h at 37°C with anti-CD39 or anti-CD73 Abs and activated for 3 to 5 days by addition of anti-CD3/anti-CD28-coated beads. Inhibition of T cell proliferation was achieved by addition of 200 μM ATP (CD39 analysis) or AMP (CD73 analysis). T cell proliferation and the ability of Abs to block the immune suppressive effect of AMP were assessed by flow cytometry by quantifying the dye dilution on proliferating T cells. Percentage of proliferating T cells versus anti-CD73 Ab concentration is plotted on graphs using GraphPad Prism software. Some experiments were

done on whole PBMC from healthy donors or cancer patients. Protocol is as described above except that T cell suppression was achieved by addition of 0.5 to 1 mM ATP.

In order to compare donors or patients, T cell proliferation was normalized using the following formula:

$$\frac{(Activated\ \ cells + AT(M)P + Ab) - (Activated\ cells + AT(M)P)}{(Activated\ cells) - (Activated\ cells + AT(M)P)} \times 100$$

Allogeneic mixed Lymphocyte Reaction (MLR) assay

Mononuclear cells from healthy donors (EFS Marseille) were isolated on a Ficoll gradient and monocytes were purified by immunomagnetic selection using CD14 microbeads (Miltenyi Biotec). Monocytes were differentiated into dendritic cells (MoDC) by 5-7 days of culture in presence of GM-CSF (400 ng/ml) and IL-4 (20 ng/ml). The day of DC recovery, $CD4^+$ T cells from allogeneic donors were purified by immunomagnetic depletion of non-$CD4^+$ T cells (Miltenyi Biotec) and stained with Cell Trace Violet. DC (10^4 cells/well) and T cells ($5x10^4$ cells/well) were mixed in 96W round bottom microplates in presence of a dose-ranges of anti-huCD73 Abs and a fixed dose of ATP. T cell proliferation and Ab ability to reverse ATP-mediated suppression was assessed as described for T cell proliferation assay. In some experiments, MoDC were activated 24 hour with ATP in presence of anti-CD39 Abs, extensively washed and incubated with allogeneic $CD4^+$ T cells as described above.

CD39 effect on inflammasome pathway

Purified monocytes were differentiated into M1-like macrophages (M1) by 7 days of culture in presence of GM-CSF (400 ng/ml). Cells were incubated with 10 μg/ml anti-CD39 Abs (1 hour, 37°C), then stimulated with 10 ng/ml LPS (3 h, 37°C) before addition of ATP (2 h, 37°C). IL-1beta was quantified by ELISA in cell culture supernatant following provider recommendations. IL-1beta concentration versus ATP concentration was plotted on graph using GraphPad Prism software.

Protein expression and purification for crystallization study

CD73 and IPH5301 Fab were produced in CHO mammalian cells and purified from culture supernatant fraction on immobilized metal ion affinity chromatography using a 5 mL HisTrap Excel (GE Healthcare) Ni2+- chelating column equilibrated in buffer A (20mM HEPES pH7.5, 150mM NaCl, 10mM imidazole). The protein was eluted with buffer A supplemented with 250mM imidazole and was further purified by a size exclusion chromatography (HiLoad 16/60 Superdex 200 prep grade, GE) equilibrated in 20mM HEPES pH7.5, 150mM NaCl. Purity of the protein was monitored using SDS–PAGE and visualized by Coomassie blue staining. The complex between CD73 and IPH5301 Fab was digested with PNGase F (sigma-Aldrich) at ratio of 1nmol:1U in size exclusion buffer at 37°C for 16 h. After digestion, size exclusion chromatography was performed with Superdex S200 Hiload 16/60 (GE Healthcare) in 20mM HEPES pH7.5, 150mM NaCl. In order to improve the homogeneity of sample, a ion exchange chromatography (MonoS 4.6/10 PE, GE Healthcare) was added. The protein concentration was determined by the absorbance of the sample at 280nm using a NanoDrop 2000. The complex between CD73 and IPH53 IgG was analyzed by size exclusion chromatography performed with Superose 6-Increase 5/150 GL (GE Healthcare) in 20mM HEPES pH7.4, 150mM NaCl, 3%Glycerol.

Negative Staining of CD73-IPH5301 complex

6 μL of a purified CD73-IPH5301 complex at 0.01 mg/mL were deposited onto a glow-discharged carbon-coated grid (Formwar/Carbon 300 mesh Cu, Agar Scientific) using a PELCO easiGlow Glow Discharge Cleaning System (Ted Pella Inc., USA). Current: 25 mA, time: 25 s and incubated for one minute. Sample excess was blotted off, rinsed with two 20 μL drops of water and stained with 10 μL of 0.75% uranyl formate for 30 s. Micrographs (100) were recorded on a Veleta 2K x 2K CCD camera using a Tecnai T12 Spirit electron microscope (FEI Company) operated at 120 kV and a magnification of 130,0003 (resulting in a pixel size of 3.46 Å/pixel). The alignment procedure was done iteratively and was considered completed when overall image shifts and rotations no longer decrease upon further alignment cycles. The aligned images were then subjected to classification. After specifying into how many classes the images should be sorted, the images in each class were averaged to create class averages. The 2D class averages are calculated by refine2D.py software in the EMAN package (Ludtke et al., 1999).

Crystallization, data collection and processing

Initial crystallization trials for CD73-IPH5301 were performed by the sitting-drop vapor-diffusion method at 293K in 96-well Swissci plates using a Mosquito Crystal robot (TTP Labtech) with the following screens: Pact Premier Screen (Molecular Dimensions), Wizard I and II (Emerald BioSystems), JCSG+ Suite (QIAGEN), LMB screen (Molecular Dimensions), Morpheus (Molecular Dimensions) Ammonium sulfate Suite (QIAGEN) and Index (Hampton Research). Crystallization hit for the complex CD73-IPH5301 (16.5mg/mL) occurred in condition No. G7 of the JCSG+ [15% PEG 3350, 0.1M succinic acid pH7]. After optimization (Lartigue et al., 2003), the final crystallization conditions were 0.1M succinic acid pH6.5-7.5, 10%–20% (w/v) PEG 3350. Crystals were briefly soaked in crystallization solution supplemented with 30% (v/v) glycerol. Diffraction data were collected to 2.78 Å resolution on beamline Proxima-1 at SOLEIL, Paris, France. The datasets were integrated with XDS (Kabsch, 2010) and were scaled with SCALA (Evans, 2006) from CCP4 Suite (Winn et al., 2011). Data collection statistics are reported in Table S4.

Structure determination

The structure of the complex CD73-IPH5301 was solved by molecular replacement with MOLREP (Vagin and Teplyakov, 2010) using the structure of human CD73 (PDB: 4H1S, closed form) and the Fab contained in the PDB: 3T2N as starting models. Refinement was performed with autoBUSTER (Blanc et al., 2004) and the structures were corrected with COOT (Emsley et al., 2010). Refinement statistics are reported in Table S4.

ELISA to assess recognition of CD39 and CD39-like proteins

1 μg/ml of recombinant human CD39 or CD39L proteins (all from Bio-Techne) were coated on MaxiSorp ELISA plates (Nunc) in PBS, overnight at 4°C. Plates were washed 5 times in washing buffer (PBS, 0.05% Tween20) and unspecific sites were saturated by adding 200 μl/w TBS starting block buffer (ThermoFisher Scientific). A dose-range of anti-CD39 antibodies was added and incubated for 2 hours at RT. Plates were washed 5 times in washing buffer and HRP-conjugated goat anti-human or goat anti-mouse IgG Fc fragment secondary Ab (bethyl) was added for 1 hour at RT to detect bound anti-CD39 Abs. Plates were washed 5 times in washing buffer and bound secondary Ab was revealed by adding TMB (HRP substrate) and incubating plates for 5 to 10 min at RT in the dark. Enzymatic reaction was stopped by adding HCl 1 M and optical density (OD) at 450 nm was measured on Enspire plate reader. OD versus anti-CD39 Ab concentration was plotted on graphs and EC_{50} was calculated using GraphPad Prism software.

SPR analysis to assess Ab KD on recombinant CD39 or CD73 proteins

SPR measurements were performed on a Biacore T200 apparatus at 25°C. Protein-A was immobilized on a Sensor Chip CM5. The chip surface was activated with EDC/NHS amine coupling kit. Protein-A was diluted to 10 μg/ml in coupling buffer (10 mM acetate, pH 5.6) and injected until the appropriate immobilization level was reached (i.e., 2000 RU). Deactivation of the remaining activated groups was performed using 100 mM ethanolamine pH 8 (GE Healthcare). Affinity study was carried out according to a standard Capture-Kinetic protocol recommended by the manufacturer (GE Healthcare kinetic wizard). Serial dilutions of human recombinant soluble CD39 or CD73 proteins, ranging from 1.23 to 300 nM were sequentially injected over the captured anti-CD39 or anti-CD73 antibodies and allowed to dissociate for 10 min before regeneration. The entire sensorgram sets were fitted using the 1:1 kinetic binding model. Monovalent affinities (CD39) and bivalent affinities (CD73) and kinetic association and dissociation rate constants are calculated.

QUANTIFICATION AND STATISTICAL ANALYSIS

Statistical analyses were performed with the non-parametric Mann-Whitney test for comparisons of two unpaired groups, the Wilcoxon t test for comparisons of two paired groups, the Kruskal-Wallis test followed by a Dunn's multiple comparisons test for comparisons of multiple unpaired groups and Kaplan-Meier test for survival analyses. Statistical analyses were performed with Prism 7 software. Differences between groups were considered statistically significant if $p < 0.05$.

DATA AND SOFTWARE AVAILABILITY

The accession number for the structure of human CD73 in complex with IPH5301 Fab reported in this paper is PDB: 6HXW.